Li et al. (2012), *The Journal of Experimental Biology*, **215**, 3293–3308. doi:10.1242/jeb.061937

Multi-functional foot use during running in the zebra-tailed lizard (*Callisaurus draconoides*)

Chen Li[1], S. Tonia Hsieh[2], and Daniel I. Goldman[1*]

[1]*School of Physics, Georgia Institute of Technology, Atlanta, GA 30332, USA and*
[2]*Department of Biology, Temple University, Philadelphia, PA 19122, USA*

[*]Author for correspondence (daniel.goldman@physics.gatech.edu)

Summary

A diversity of animals that run on solid, level, flat, non-slip surfaces appear to bounce on their legs; elastic elements in the limbs can store and return energy during each step. The mechanics and energetics of running in natural terrain, particularly on surfaces that can yield and flow under stress, is less understood. The zebra-tailed lizard (*Callisaurus draconoides*), a small desert generalist with a large, elongate, tendinous hind foot, runs rapidly across a variety of natural substrates. We use high speed video to obtain detailed three-dimensional running kinematics on solid and granular surfaces to reveal how leg, foot, and substrate mechanics contribute to its high locomotor performance. Running at ~ 10 body length/s (~ 1 m/s), the center of mass oscillates like a spring-mass system on both substrates, with only 15% reduction in stride length on the granular surface. On the solid surface, a strut-spring model of the hind limb reveals that the hind foot saves about 40% of the mechanical work needed per step, significant for the lizard's small size. On the granular surface, a penetration force model and hypothesized subsurface foot rotation indicates that the hind foot paddles through fluidized granular medium, and that the energy lost per step during irreversible deformation of the substrate does not differ from the reduction in the mechanical energy of the center of mass. The upper hind leg muscles must perform three times as much mechanical work on the granular surface as on the solid surface to compensate for the greater energy lost within the foot and to the substrate.

Key words: terrestrial locomotion, mechanics, energetics, kinematics, spring-mass system, elastic energy savings, dissipation, granular media

Running title: Substrate effects on foot use in lizards

Introduction

Rapid locomotion like running and hopping can be modeled as a spring-mass system bouncing in the sagittal plane (i.e., the Spring-Loaded Inverted Pendulum model, SLIP) (Blickhan, 1989). This has been demonstrated in a variety of animals (Blickhan and Full, 1993; Holmes et al., 2006) in the laboratory on rigid, level, flat, non-slip surfaces (hereafter referred to as "solid surfaces") such as running tracks and treadmills (Dickinson et al., 2000). In the SLIP model, the animal body (represented by the center of mass, CoM) bounces on a single leg (represented by a spring) like a pogo stick, and exerts point contact on the solid ground. The leg spring compresses during the first half of stance, and then recoils during the second half of stance. Through this process, the mechanical (i.e., kinetic plus gravitational potential) energy of the CoM is exchanged with elastic energy stored in the compressed leg spring, reducing energy use during each step. For animals like insects (e.g., Schmitt et al., 2002) and reptiles (e.g., Chen et al., 2006) that run with a sprawled limb posture, the CoM also oscillates substantially in the horizontal plane in a similar fashion, which can also be modeled as a spring-mass system bouncing in the horizontal plane (i.e., the Lateral Leg Spring model, LLS) (Schmitt et al., 2002). Both the SLIP and the LLS models predict that the mechanical energy of the CoM is lowest at mid-stance and highest during aerial phase.

In these models, the spring-mass system and the interaction with the solid ground are perfectly elastic and do not dissipate energy; thus no net work is performed. However, as animals move across natural surfaces, energy is dissipated both within their body and limbs (Fung, 1993) and to the environment (Dickinson et al., 2000). Therefore, mechanisms to reduce energy loss during locomotion can be important. The limbs of many organisms possess elastic elements such as tendons and ligaments that can function as springs to store and return energy during rapid locomotion like running and hopping to decrease energetic cost (Alexander, 2003). Most notable for this function are the ankle extensor tendons in the lower hind leg and the digital flexor tendons and ligaments in the lower fore leg (Alexander, 2003). Furthermore, different limb-ground interaction strategies may be utilized depending on the dissipative properties of the substrate.

Laboratory experiments have begun to reveal mechanisms of organisms running on non-solid surbstrates, such as elastic (Ferris et al., 1998; Spence et al., 2010), damped (Moritz and Farley, 2003), inclined (Roberts et al., 1997), or uneven (Daley and Biewener, 2006; Sponberg and Full, 2008) surfaces; surfaces with few footholds (Spagna et al., 2007); and the surface of water (Glasheen and McMahon 1996a; Hsieh, 2003). While spring-mass-like CoM motion was

observed only in some of these studies (Ferris et al., 1998; Moritz and Farley, 2003; Spence et al., 2010), a common finding is that on non-solid surfaces limbs do not necessarily behave like springs to save energy. In addition, these studies suggest that both the active control of body and limb movement through the nervous system, and the passive mechanical responses of viscoelastic limbs and feet with the environment, play important roles in the control of rapid terrestrial locomotion (for reviews, see Full and Koditschek, 1999; Dickinson et al., 2000).

Many substrates found in nature, such as sand, gravel, rubble, dirt, soil, mud, and debris, can yield and flow under stress during locomotion and experience solid-fluid transitions, through which energy may be dissipated via plastic deformation. Understanding locomotion on these substrates is challenging in part because, unlike for flying and swimming where the fluid flows and forces can in principle be determined by solving the Navier-Stokes equations in the presence of moving boundary conditions (Vogel, 1996), no comprehensive force models yet exist for terrestrial substrates that yield and flow (hereafter referred to as "flowing substrates").

Granular materials (Nedderman, 1992) like desert sand which are composed of similarly sized particles provide a good model substrate for studying locomotion on flowing substrates. Compared to other flowing substrates, granular materials are relatively simple and the intrusion forces within them can be modeled empirically (Hill et al., 2005). Their mechanical properties can also be precisely and repeatedly controlled using a fluidized bed (Li et al., 2009). In addition, locomotion on granular surfaces is directly relevant for many desert-dwelling reptiles and arthropods such as lizards, snakes, and insects (Mosauer, 1932; Crawford, 1981). Recent advances in the understanding of force and flow laws in granular materials subject to localized intrusion (Hill et al., 2005; Katsuragi and Durian, 2007; Gravish et al., 2010; Ding et al., 2011a) begin to provide insight into the mechanics of locomotion on (and within) granular substrates (Li et al., 2009; Maladen et al., 2009; Mazouchova et al., 2010; Li et al., 2010b; Maladen et al., 2011; Ding et al., 2011b; Li et al., in press).

The zebra-tailed lizard (*Callisaurus draconoides*, SVL ~ 10 cm, mass ~ 10 g, Fig. 1A) is an excellent model organism for studying running on natural surfaces, because of its high locomotor performance over diverse terrain. As a desert generalist, this lizard lives in a range of desert habitats including flat land, washes, and sand dunes (Vitt and Ohmart, 1977; Korff and McHenry, 2011), and encounters a large variety of substrates ranging from rocks, gravel, closely-packed coarse sand, and loosely-packed fine sand (Karasov and Anderson, 1998; Korff and McHenry, 2011). The zebra-tailed lizard is the fastest-running species among desert lizards of similar size

(Irschick and Jayne, 1999a), and has been observed to run at up to 4 m/s (50 bl/s) both on solid (e.g., treadmill) (Irschick and Jayne, 1999a) and on granular (e.g., sand dunes) (Irschick and Jayne, 1999b) surfaces. Its maximal acceleration and running speed also did not differ significantly when substrate changes from coarse wash sand to fine dune sand, whose yield strengths differ by a factor of three (Korff and McHenry, 2011).

Of particular interest is whether and how the zebra-tailed lizard's large, elongate hind foot contributes to its high locomotor capacity. In addition to a slim body, a long tapering tail, and slender legs (Fig. 1A), the zebra-tailed lizard has an extremely large, elongate hind foot, the largest (40% SVL) among lizards of similar size (Irschick and Jayne, 1999a). Its hind foot is substantially larger than the fore foot (area = 1 cm^2 vs. = 0.3 cm^2) and likely plays a dominant role for locomotion (Mosauer, 1932). Recent studies in insects, spiders, and geckos (Jindrich and Full, 1999; Antumn et al., 2000; Dudek and Full, 2006; Spagna et al., 2007) suggested that animals can rely on appropriate morphology and material properties of their bodies and limbs to accommodate variable, uncertain conditions during locomotion. Despite suggestions that the large foot area (Mosauer, 1932) and increased stride length via elongate toes may confer locomotor advantages (Irschick and Jayne, 1999a), the mechanisms of how the hind foot contributes to the zebra-tailed lizard's high running capacity remain unknown.

In this paper, we study the mechanics and mechanical energetics of the zebra-tailed lizard running on two well-defined model surfaces, a solid surface and a granular surface. These two surfaces lie on opposite ends of the spectrum of substrates that the zebra-tailed lizard encounters in its natural environment, and present distinct conditions for locomotion. We investigate whether the lizard's center of mass bounces like a spring-mass system during running on both solid and granular surfaces. We combine measurements of three-dimensional kinematics of the lizard's body, hind limb, and hind foot, dissection and resilience measurements of the hind limb, and modeling of foot-ground interactions on both substrates, and demonstrate that the lizard's large, elongate hind foot serves different functions during running on solid and granular surfaces. We find that on the solid surface, the hind foot functions as an energy-saving spring; on the granular surface, it functions as a dissipative, force-generating paddle to generate sufficient lift during each step. The larger energy dissipation to the substrate and within the foot during running on the granular surface must be compensated for by greater mechanical work done by the upper hind leg muscles.

Materials and methods

Animals

Seven adult zebra-tailed lizards (*Callisaurus draconoides*) were collected from the Mojave Desert, AZ, USA in 08/2007 (Permit SP591773) for three-dimensional kinematics experiments. Table 1 shows the morphological measurements for these seven animals. Eleven additional adult animals were collected from the Mojave Desert, CA, USA in 09/2009 (Permit SC 10901) for hind limb resilience measurements. Two preserved specimens were used for dissection. The animals were housed in the Physiological Research Laboratory animal facility of The Georgia Institute of Technology. Each animal was housed individually in an aquarium filled with sand, and fed crickets and mealworms dusted with vitamin and calcium supplement two to three times a week. The ambient temperature was maintained at 28°C during the day and 24°C during the night. Full-spectrum fluorescent bulbs high in UVB were set to a 12 hour/12 hour light/dark schedule. Ceramic heating elements were provided 24 hours a day to allow the animals to thermo-regulate at preferred body temperature. All experimental procedures were conducted in accordance with The Georgia Institute of Technology IACUC protocols.

Surface treatments

A wood board (120 × 23 × 1 cm^3) bonded with sandpaper (grit size ~ 0.1 mm) for enhanced traction was used as the solid surface. Glass particles (diameter = 0.27 ± 0.04 mm mean ± 1 standard deviation, density = 2.5×10^3 kg/m^3, Jaygo Incorporated, Union, NJ, USA) were used as the granular substrate, which are approximately spherical and of similar size to typical desert sand (Dickinson and Ward, 1994). Before each trial, a custom-made fluidized bed trackway (200 cm long, 50 cm wide) prepared the granular substrate (12 cm deep) into a loosely packed state (volume fraction = 0.58) for repeatable yield strength (for experimental details of the fluidized bed trackway, see Li et al., 2009).

Three-dimensional kinematics

We used high speed video to obtain three-dimensional kinematics as the lizard ran across the prepared surfaces (Fig. 1B). Before each session, high-contrast markers (Wite-Out, Garden Grove, CA, USA) were painted on each animal for digitizing at nine joints along the midline of the trunk and the right hind limb (Fig. 1A,B): neck (N), center of mass (CoM), pelvis (P), hip (H), knee (K), ankle (A); and the metatarsal-phalangeal joint (MP), distal end of the proximal phalanx (PP), and digit tip (T) of the fourth toe. The approximate longitudinal location of the CoM in resting position was determined by tying a thread around the body of an anesthetized lizard and

repositioning the thread until the body balanced horizontally. Before each trial, the surface was prepared (for the granular surface treatment only), and calibration images were taken of a custom-made 39-point calibration object (composed of LEGO, Billund, Denmark). The animal was then induced to run across the field of view by a slight tap or pinch on the tail. Two synchronized AOS high speed cameras (AOS Technologies, Baden Daettwil, Switzerland) captured simultaneous dorsal and lateral views at 500 frame/s (shutter time = 300 μs). The ambient temperature was maintained at 35°C during the test. Animals were allowed to rest at least five minutes between trials and at least two days between sessions.

We digitized the calibration images and high speed videos, and used direct linear transformation (DLT) to reconstruct three-dimensional kinematics from the two-dimensional kinematics from both dorsal and lateral views. Digitization and DLT calculations were performed using custom software (DLTcal5 and DLTdv5, Hedrick, 2008). Axes were set such that +*x* pointed in the direction of forward motion, +*z* pointed vertically upward, and +*y* pointed to the left of the animal. Footfall patterns of touchdown and takeoff were determined from the videos. On the granular surface, because the hind foot often remained obscured by splashed grains during foot extraction, we defined foot takeoff as when the knee began to flex following extension during limb protraction (which is when foot takeoff occurs on the solid surface). To reduce noise and enable direct comparisons among different running trials, position data were filtered with a Butterworth low-pass filter with a cutoff frequency of 75 Hz, and interpolated to 0–100% of one full stride period (*T*) between two successive touchdowns of the right hind limb. All data analysis was completed with MATLAB (MathWorks, Natick, MA, USA) unless otherwise specified.

Statistics

We accepted trials that met the following criteria: the animal ran continuously through the field of view, the run was straight without contacting sidewalls of the trackway, there was a full stride (between two consecutive touchdowns of the right hind limb) in the range of view, all the nine markers were visible throughout the full stride, and the forward speed changed less than 20% after the full stride. With these criteria, out of a total of 125 trials from 7 individuals on both solid (61 trials from 7 individuals) and granular (64 trials from 7 individuals) surfaces collected over a period of over three months, we ultimately accepted 51 runs from 7 individuals on solid (23 runs from 7 individuals) and granular (28 runs from 7 individuals) surfaces. Because the data set had an unequal number of runs per individuals, and because we were measuring freely-running animals and did not control for speed, to maintain statistical power, all statistical tests were

performed on a subset of these data using one representative run per individual on both solid (N = 7) and granular (N = 7) surfaces. The representative run for each individual was selected based on having the most consistent running speed for at least one full stride and was also closest to the mean running speed of all 51 trials. Data are reported as mean ± 1 standard deviation (s.d.) from the 7 representative runs on each substrate unless otherwise specified.

To determine the effect of substrate, all kinematic variables were corrected for size-related differences by regressing the variables against SVL and taking the residuals for those that regressed significantly with SVL ($P < 0.05$). We then ran an ANCOVA with substrate and speed as covariates to test for substrate effects, independent of running speeds. All statistical tests were performed using JMP (SAS, Cary, NC, USA).

For the energetics data, we used dimensionless quantities by normalizing energies of each run to the CoM mechanical energy at touchdown of that run, thus eliminating the effect of mass and running speed on energies. An ANOVA was used to test the differences between the reduction in CoM mechanical energy, elastic energies, and energy loss. A Tukey's HSD was used for post-hoc tests where needed.

Dissection and model of hind limb

To gain insight into the role of anatomical components of the hind limb on mechanics during locomotion, we dissected the hind limb of two preserved specimens. We quantified anatomical dimensions by measuring the radii of the knee (K), ankle (A), the metatarsal-phalangeal joint (MP), the distal end of the proximal phalanx (PP), and the digit tip (T) of the fourth toe. We also observed the muscle and tendon arrangements within the lower leg and the foot. Based on these anatomical features, we developed a model of the hind limb which incorporated the structure, properties, and function of its main elements.

Resilience measurements of hind limb

To characterize the resilience of the hind limb for estimation of energy return, a modification of the work loop technique was used (Fig. 2A), in which the limb was kept intact and forces were applied to the whole limb instead of a single muscle (Dudek and Full, 2006). The animal was anesthetized using 2% isoflurane air solution during the test. The hind foot was maintained within the vertical plane, pushed down onto and then extracted from a custom force platform suited for small animals (10.2 × 7.6 cm^2, range = 2.5 N, resolution = 0.005 N) bonded with sandpaper (grit size ~ 0.1 mm). Ground reaction force F was measured at 10 kHz sampling rate using a custom

LabVIEW program (National Instruments, Austin, TX, USA). A Phantom high speed camera (Vision Research, Wayne, NJ, USA) simultaneously recorded deformation of the foot from the side view at 250 frame/s (shutter time = 500 μs). High-contrast markers (Wite-Out, Garden Grove, CA, USA) were painted on the joints of the hind foot (A, MP, PP, T, and a point on the tibia above the ankle). The ambient temperature was maintained at 35°C during the test.

Videos of foot deformation were digitized to obtain the angular displacement of the foot $\Delta\theta = \theta_0 - \theta_t$, i.e., the change in the angle formed by the tibia and the foot (from the ankle to the digit tip of the fourth toe) (Fig. 2A). Angular displacement $\Delta\theta$ was synchronized with the measured torque τ about the ankle (calculated from the measured ground reaction force) to obtain a passive work loop. The damping ratio of the hind limb, i.e., the percentage of energy lost within the hind limb after loading and unloading, was calculated as the fraction of area within a work loop relative to the area under the higher loading curve (Fung, 1993). Hind limb resilience, i.e., the percentage of energy returned by the foot after loading and unloading, was one minus the damping ratio (Ker et al., 1987; Dudek and Full, 2006). An ANOVA was used to test the effect of maximal torque, maximal angular displacement, loading rate, and individual animal on hind limb resilience.

Granular penetration force measurements

While comprehensive force models are still lacking to calculate ground reaction forces during locomotion granular media, a low speed penetration force model was previously used to explain the locomotor performance of a legged robot on granular media (Li et al., 2009). Similarly, to estimate the vertical ground reaction force on the lizard foot during running on the granular surface, we measured the vertical force on a plate slowly penetrating vertically into the granular substrate (Fig. 2B). Before each trial, a fluidized bed (area = 24 × 22 cm^2) prepared the granular substrate (depth = 12 cm) into a loosely packed state (volume fraction = 0.58) (for details, see Maladen et al., 2009). A robotic arm (CRS robotics, Burlington, OT, Canada) pushed a horizontally-oriented plate vertically downward at 0.01 m/s into the granular substrate to a depth of 7.6 cm, and then extracted the plate vertically at 0.01 m/s. The force on the plate was measured by a force transducer (ATI Industrial Automation, Apex, NC, USA) mounted between the robotic arm and the plate at 100 Hz sampling rate using a custom LabVIEW program (National Instruments, Austin, TX, USA). The depth of the plate was measured by tracking the position of an LED light marker mounted on the robotic arm in side view videos taken by a Pike high speed camera (Edmund Optics, Barrington, NJ, USA). Two thin aluminum plates of different area were

used (A_1 = 7.6 × 2.5 cm^2 and A_2 = 3.8 × 2.5 cm^2; thickness = 0.6 cm). Three trials were performed for each plate.

Results

Performance and gait

On both solid and granular surfaces, the zebra-tailed lizard ran with a diagonal gait, a sprawled limb posture, and lateral trunk bending (see Fig. 3 and Movies 1, 2 in supplementary material for representative runs on both substrates). Figure 4 shows average forward speed $\bar{v}_{x,\mathrm{CoM}}$, stride frequency f, and duty factor D of the entire data set (all symbols; 23 runs on the solid surface and 28 runs on the granular surface) and of the representative runs (filled symbols; N = 7 on the solid surface and N = 7 on the granular surface). Table 2 lists mean values and statistical results for all the gait and kinematic variables from the representative runs for both solid (N = 7) and granular (N = 7) surfaces. On both surfaces, $\bar{v}_{x,\mathrm{CoM}}$ increased with f (Fig. 4A, $P < 0.05$, ANCOVA), and D decreased with $\bar{v}_{x,\mathrm{CoM}}$ (Fig. 4B, $P < 0.05$, ANCOVA). $D \approx 0.45$ on both surfaces resulting in an aerial phase of approximately 5% stride period T between alternating stances (Fig. 5A). Neither $\bar{v}_{x,\mathrm{CoM}}$ ($P > 0.05$, ANOVA) nor D ($P > 0.05$, ANCOVA) significantly differ between surfaces. Average stride length $\lambda = \bar{v}_{x,\mathrm{CoM}}/f$ was 15% shorter on the granular surface ($P < 0.05$, ANCOVA).

Center of mass kinematics

The lizard displayed qualitatively similar center of mass oscillations during running on both surfaces. The CoM forward speed $v_{x,\mathrm{CoM}}$ (Fig. 5B) and vertical position z_{CoM} (Fig. 5C) oscillated at 2f, dropping during the first half and rising during the second half of a stance, i.e., reaching minimum at mid-stance and maximum during the aerial phase. The CoM also oscillated medio-laterally at f (Fig. 5D). Throughout the entire stride, z_{CoM} was significantly higher on the solid surface ($P < 0.05$, ANCOVA). The CoM vertical oscillations Δz_{CoM} and lateral oscillations Δy_{CoM} did not differ between substrates ($P > 0.05$, ANCOVA).

Hind foot, hind leg, and trunk kinematics

The lizard displayed distinctly different hind foot, hind leg, and trunk kinematics during running on solid and granular surfaces (Figs. 3, 6). On the solid surface, the lizard used a digitigrade foot posture (Fig. 3A–E, solid line/curve). During the entire stride, the hind foot engaged the solid

surface only with the digit tips. At touchdown, the toes were straight and pointed slightly downward. The touchdown foot angle (measured along the fourth toe) was $\theta_{touchdown} = 12 \pm 4°$ relative to the surface (Fig. 3A,E; Fig. 6A, red). During stance, the long toes pivoted over the stationary digit tips (Fig. 3A–C, vertical dotted line shows zero displacement) and hyperextended into a c-shape (Fig. 3B, solid curve). The foot straightened again at takeoff, pointing downward and slightly backward (Fig. 3C, solid line), and then flexed during swing (Fig. 3D, solid curve).

On the granular surface, the lizard used a plantigrade foot posture (Fig. 3F,J, solid line). At touchdown, the hind foot was nearly parallel with the surface, with the toes spread out and held straight. In the vertical direction, the foot impacted the granular surface at speeds of up to 1 m/s. The ankle joint slowed down to ~ 0.1 m/s within a few milliseconds following impact (a few percent of stride period *T*) while the the foot started penetrating the surface. The touchdown foot angle was $\theta_{touchdown} = 4 \pm 3°$ relative to the surface (Fig. 3J; Fig. 6A, blue), significantly smaller than that on the solid surface ($P < 0.05$, ANCOVA). During stance, the entire foot moved subsurface and was obscured (Fig. 3G). The ankle joint remained visible right above the surface and moved forward by about a foot length (Fig. 3F–H, vertical dotted line shows ankle displacement). The foot was extracted from the substrate at takeoff, pointing downward and slightly backward, and then flexed during swing (Fig. 3I, solid curve).

As a result of foot penetration on the granular surface, both the knee height z_{knee} (Fig. 6B) and pelvis height z_{pelvis} (Fig. 6C) were lower on the granular surface ($P < 0.05$, ANCOVA). In addition, on the granular surface, the knee moved downward by a larger vertical displacement Δz_{knee} during the first half of stance ($P < 0.05$, ANCOVA; Fig. 6B), while the knee joint extended by a larger angle $\Delta\theta_{knee}$ during the second half of stance ($P < 0.05$, ANCOVA; Fig. 6D). Throughout the entire stride, the trunk was nearly horizontal on the solid surface (Fig. 3A–D, dashed line), but pitched head-up on the granular surface (Fig. 3F–I, dashed line; Fig. 6E). On both surfaces, the hind legs were sprawled at an angle of $\theta_{sprawl} \approx 40°$ during stance (Fig. 3; θ_{sprawl} is defined as the angle between the horizontal plane and the leg orientation in the posterior view). In most runs, the tail was farther from the solid surface and closer to the granular surface (Fig. 3).

Hind limb anatomy

From morphological measurements (Table 1), the hind foot of the zebra-tailed lizard comprised 42% of the hind limb length, and the longest fourth toe alone accounted for 63% of the hind foot length. These ratios are in similar range to previous observations (Irschick and Jayne, 1999a). The

slender foot had a cross-sectional radius of r = 0.50–1.25 mm tapering distally, with reducing joint radii: $r_K = r_A$ = 1.25 mm, r_{MP} = 0.75 mm, $r_{PP} = r_T$ = 0.50 mm.

Unlike many cursorial mammals whose ankle extensor muscles of the lower hind leg have long tendons (Alexander, 2003), ankle extensor tendons are nearly non-existent in the zebra-tailed lizard (Fig. 7A). Instead, layers of elongate tendons were found in both the dorsal and ventral surfaces of the foot. Our anatomical description is focused on the ventral muscle and tendon anatomy in the hind limb and terms given to muscles and tendons follow (Russell, 1993). A large, tendinous sheath, the superficial femoral aponeurosis, originates from the femoro-tibial gastrocnemius, stretches across the ventral surface of the foot, and inserts on the metatarsal-phalangeal joints for digits III and IV. The superficial portion of the femoro-tibial gastrocnemius muscle body extends to the base of the ankle, thereby rendering the human equivalent of the ankle extensor tendons (i.e., the "Achilles" tendon) absent. Deep to the superficial femoral aponeurosis lie the flexor digitorum brevis muscles (not shown) which control the flexion of each of the digits. Tendons from the flexor digitorum longus muscle located on the lower hind leg run deep to the flexor digitorum brevis muscle bodies, and extend to the tips of the digits. No additional tendons are visible deep to the flexor digitorum longus tendons.

Hind limb model

Based on the observed muscle and tendon anatomy, we propose a two-dimensional strut-spring model of the hind limb (Fig. 7B), which assumes isometric contraction for the lower leg muscles and incorporates the spring nature of the foot tendons. This model is inspired from previous observations in large running and hopping animals of the strut-like function of ankle extensor muscles (Biewener, 1998a; Roberts et al., 1997) and spring-like function of ankle extensor tendons (for a review, see Alexander, 2003). Rigid segments (Fig. 7B, dashed lines), which are free to rotate about joints within a plane, represent the skeleton. The ankle extensor muscles in the lower leg, which originate on the femur and run along the ventral side of the tibia, are modeled as a rigid strut (muscle strut, Fig. 7B, blue line) that contracts isometrically during stance in running. A linear spring (tendon spring, Fig. 7B, red line), which originates from the distal end of the muscle strut and extends to the digit tip, models the elastic foot tendons. The muscle strut and tendon spring are ventrally offset from the midline of the skeleton at each joint by respective joint radii.

Hind limb resilience

Representative passive work loops (Fig. 8A–C) showed that torque τ was higher when the foot was pushed down on the solid surface than when it was extracted, similar to previous observations in humans (Ker et al., 1987) and cockroaches (Dudek and Full, 2006). Maximal torque was positively correlated with maximal angular displacement ($F_{1,62}$ = 64.3188, $P < 0.001$, ANOVA). The kinks observed in the middle of the loading curve were due to the fifth toe contacting the surface. Average hind limb resilience calculated from the work loops was $R = 0.44 \pm 0.12$ (Fig. 8D–F, 3 individuals, 64 trials). R did not differ between individuals ($F_{2,61}$ = 2.1025, P = 0.1309, ANOVA), and did not depend on maximal torque ($F_{1,62}$ = 0.5208, P = 0.4732, ANOVA; Fig. 8D), maximal angular displacement ($F_{1,62}$ = 0.0164, P = 0.8987, ANOVA; Fig. 8E), or average loading rate ($F_{1,62}$ = 1.1228, P = 0.2934, ANOVA; Fig. 8F).

Hind foot curvature, tendon deformation, and tendon stiffness

The observed three-dimensional positions of the hind limb fit well to the two-dimensional hind limb model (Fig. 9A–D), and enabled calculation of the curvature, tendon deformation, and tendon stiffness of the hind foot (see Appendix). Calculated hind foot curvature κ (Fig. 9E, solid curve) showed that the hind foot hyperextended during stance (positive κ) and flexed during swing (negative κ). The foot was straight at touchdown and shortly after takeoff ($\kappa = 0$). Calculated tendon spring deformation Δl (Fig. 9E, dashed curve) showed that the tendon spring stretched during the first half and recoiled during the second half of stance. The estimated tendon spring stiffness was $k = 4.4 \times 10^3$ N/m (see Appendix).

Mechanical energetics on solid surface

Using the observed CoM and hind limb kinematics, calculated tendon spring stiffness and deformation, and measured hind limb resilience, we examined the mechanical energetics of the lizard running on the solid surface (Table 3, Fig. 9F). From the observed CoM kinematics, in the first half of stance, the mechanical energy of the CoM (kinetic energy plus gravitational potential energy) decreased significantly from $E_{\text{touchdown}} = 1.00 \pm 0.00$ at touchdown to $E_{\text{mid-stance}} = 0.81 \pm 0.08$ at mid-stance ($F_{2,18}$ = 12.2345, P = 0.0004, ANOVA, Tukey HSD). In the second half of stance, the mechanical energy of the CoM recovered to $E_{\text{aerial}} = 0.95 \pm 0.10$ at mid aerial phase, not significantly different from $E_{\text{touchdown}}$ (Tukey HSD). The reduction in CoM mechanical energy in the first half of stance $\Delta E_{\text{mech}} = 0.19 \pm 0.08$ is the mechanical work needed per step on the solid surface. Note that the energies of each run were normalized to $E_{\text{touchdown}}$ of that run.

At mid-stance, the elastic energy stored in the tendon spring was $E_{storage} = 0.18 \pm 0.13$ (calculated from $1/2\ k\Delta l_{max}^2$, see Appendix), not significantly different from ΔE_{mech} ($F_{1,12} = 0.0475$, $P = 0.8312$, ANOVA). Because hind limb resilience $R = 0.44 \pm 0.12$, the elastic recoil of the foot tendons returned an energy of $E_{return} = RE_{storage} = 0.08 \pm 0.06$, or $41 \pm 33\%$ of the mechanical work needed per step (ΔE_{mech}) on the solid surface. We verified that foot flexion during swing induced little energy storage ($< 0.1\ E_{storage}$) because the hind foot was less stiff during flexion (0.7×10^3 N/m) than during hyperextension (4.4×10^3 N/m).

Granular penetration force model

Although little is known about the kinematics and mechanics of the complex limb intrusions during legged locomotion on granular surfaces, we took inspiration from previous observations that horizontal drag (Maladen et al., 2009) and vertical impact (Katsuragi and Durian, 2007) forces in glass particles were insensitive to speed when intrusion speed was below approximately 0.5 m/s. Because the kinematics observed on the granular surface suggest that the vertical speeds of most of the foot relative to the ground were below 0.5 m/s during most of the stance phase (see Appendix), we assumed that the ground reaction forces on the lizard's feet were also insensitive to speed. This allowed us to use the vertical penetration force measured at 0.01 m/s to model and estimate the vertical ground reaction forces on the lizard foot.

From the force data on both plates (Fig. 10), vertical ground reaction force F_z was proportional to both penetration depth $|z|$ and projected area A of the plate (area projected into the horizontal plane). F_z was pointing upward during foot penetration, and pointing downward during foot extraction and dropped by an order of magnitude. These measurements were in accord with previous observations of forces on a sphere penetrating into granular media (Hill et al., 2005). Furthermore, we estimated from free falling of particles under gravity that it would take longer than the stance duration (45 ms) for the grains surrounding a penetrating foot to refill a hole created by the foot of maximal depth ($|z|_{max} = 1.0$ cm, see Appendix). Thus we assumed that the vertical ground reaction forces were negligible during foot extraction.

Therefore, we approximate the vertical penetration force as:

$$F_z = \begin{cases} \alpha |z| A, & \text{for increasing } |z|, \\ 0, & \text{for decreasing } |z|, \end{cases} \qquad (1)$$

where α is the vertical stress per unit depth, which is determined by the properties of the granular material and increases with compaction (Li et al., 2009). Fitting $F_z = \alpha |z| A$ to the force data

during penetration over regions where the plate was fully submerged and far from boundary (Fig. 10, dashed lines), we obtained $\alpha = 3.5 \times 10^5$ N/m^3 for loosely packed 0.27 ± 0.04 mm diameter glass particles.

Vertical ground reaction force on granular surface

During a stance on the granular surface, the CoM vertical speed $v_{z,CoM}$ (calculated from z_{CoM}) was approximately sinusoidal (Fig. 11A, dashed curve). This implies that the F_z on a lizard foot must be approximately sinusoidal. In addition, the foot was nearly horizontal at touchdown, but pointed downward and slightly backward during takeoff. In consideration of the functional form of the penetration force (Eqn. 1), we hypothesized that during stance the foot rotated subsurface by $\pi/2$ in the sagittal plane (Fig. 11C), increasing foot depth $|z|$ but decreasing projected foot area A, thus resulting in a sinusoidal F_z which reaches a maximum at mid-stance before the foot reaches largest depth (see Appendix). A sinusoidal F_z is also possible for a fixed projected foot area if the foot maintains contact on solidified grains. However, this is unlikely considering that during stance the ankle moved forward at the surface level by a foot length.

Assuming that during stance the hind foot rotated by $\pi/2$ in the sagittal plane at a constant angular velocity, the vertical ground reaction force that each foot generated was $F_z = 5\pi mg/9 \sin 10\pi t/9T$ (see Appendix). The net vertical acceleration due to this F_z and the animal weight mg was $a_z = F_z/m - g$ (Fig. 11B; solid and dashed curves are a_z from both hind feet, shifted from each other by $T/2$). The CoM vertical speed $v_{z,CoM}$ predicted from the total a_z on both hind feet (Fig. 11A, dashed curve) agreed with experimental observations (Fig. 11A, solid curve). The slight under-prediction of the oscillation magnitudes of $v_{z,CoM}$ was likely due to an over-estimation of duty factor on the granular surface. This is because F_z may have dropped to zero even before takeoff if the foot started moving upward before takeoff (Fig. 10).

Mechanical energetics on granular surface

Using the measured CoM kinematics, assumed foot rotation, and calculated vertical ground reaction force, we examined the mechanical energetics of the lizard running on the granular surface (Table 3, Fig. 11D). In the first half of stance, the mechanical energy of the CoM decreased significantly from $E_{touchdown} = 1.00 \pm 0.00$ at touchdown to $E_{mid\text{-}stance} = 0.86 \pm 0.09$ at mid-stance ($F_{2,18} = 6.6132$, $P = 0.007$, ANOVA, Tukey HSD). In the second half of stance, the mechanical energy of the CoM recovered to $E_{aerial} = 0.99 \pm 0.10$ at mid aerial phase, not significantly different from $E_{touchdown}$ (Tukey HSD). The reduction in CoM mechanical energy in

the first half of stance ΔE_{mech} = 0.14 ± 0.09 is the mechanical work needed per step on the granular surface. By integration of F_z over vertical displacement of the foot during stance (see Appendix), the energy lost to the granular substrate per step was estimated as $E_{substrate}$ = 0.17 ± 0.05, not significantly different from ΔE_{mech} ($F_{1,12}$ = 0.4659, P = 0.5078, ANOVA). Note that the energies of each run were normalized to $E_{touchdown}$ of that run.

Discussion

Conservation of spring-mass-like CoM dynamics on solid and granular surfaces

The observed kinematics and calculated mechanical energetics demonstrated that the zebra-tailed lizard ran like a spring-mass system on both solid and granular surfaces. On both surfaces, the CoM forward speed (Fig. 5B), vertical position (Fig. 5C), and lateral position (Fig. 5D) displayed oscillation patterns that are in accord with predictions from the Spring-Loaded Inverted Pendulum (SLIP) model (Blickhan, 1989) and the Lateral Leg Spring (LLS) model (Schmitt et al., 2002). The small relative oscillations of the CoM forward speed (i.e., $\Delta v_{x,CoM}/v_{x,CoM} << 1$) was expected because the Froude number was large for the lizard (see Appendix). The substantial sprawling of the legs contributed to the medio-lateral oscillatory motion of the animal. Furthermore, on both surfaces, the mechanical energy of the CoM oscillated within a step, reaching minimum at mid-stance and maximum during the aerial phase (Fig. 9F, 11D), a defining feature of spring-mass like running (Blickhan, 1989; Schmitt et al., 2002).

To our knowledge, ours is the first study to quantitatively demonstrate spring-mass-like CoM motion in lizards running on granular surfaces. Spring-mass-like CoM motion was previously observed in other lizards and geckos running on solid surfaces (Farley and Ko, 1997; Chen et al., 2006), but it was not clear whether energy-saving by elastic elements played an important role.

Hind foot function on solid surface: energy-saving spring

Our study is also the first to quantify elastic energy savings in foot tendons in lizards during running on solid surfaces. The significant energy savings (about 40% of the mechanical work needed per step) in the zebra-tailed lizard's hind foot tendons is in a similar range to the energy savings by ankle extensor tendons and digital flexor tendons and ligaments in larger animals (Alexander, 2003), such as kangaroos (50%, Alexander and Vernon, 1975), wallabies (45%,

Biewener et al., 1998), horses (40%, Biewener, 1998b), and humans (35%, with an additional 17% from ligaments in the foot arch, Ker et al., 1987).

This is surprising considering that the elastic energy saving mechanism was previously thought less important in small animals (e.g., 14% in hopping kangaroo rat of ~ 100 g mass, Biewener et al., 1981). Because the tendons of small animals are "overbuilt" to withstand large stresses during escape, during steady-speed locomotion these tendons usually experience stresses too small to induce significant elastic energy storage and return (Biewener and Blickhan, 1988; McGowan et al., 2008). We verified that for zebra-tailed lizards running at ~ 1 m/s the maximal stress in the foot tendons is 4.3 MPa (see Appendix), well below the 100 MPa breaking stress for most tendons (Kirkendall and Garrett, 1997).

The zebra-tailed lizard's elongate hind foot and digitigrade foot posture on the solid surface may be an adaptation for elastic energy saving during rapid locomotion. Like other iguanids (Russell, 1993), this lizard does not have substantial ankle extensor tendons as large animals do. Nevertheless, elongation of foot tendons and a digitigrade posture enhance the hind foot's energy saving capacity by decreasing tendon stiffness and mechanical advantage (Biewener et al., 2004) (see Appendix). A recent study also found significant energy savings (53%) by elongate foot tendons in running ostriches (Rubenson et al., 2011). More generally, elongation of distal limb segments such as legs, feet, and toes which possess tendons may be an adaptation for energy saving during rapid locomotion. Indeed, many cursorial animals including mammals (Garland Jr. and Janis, 1993), lizards (Bauwens et al., 1995), and dinosaurs (Coombs Jr., 1978) display elongation of distal limb segments. Short fascicles and long tendons and ligaments are often found in the ankle extensor muscles and digital flexor muscles in large cursorial ungulates such as horses, camels, and antelopes (Alexander, 2003).

Solid surface model assumptions

Our estimates of elastic energy storage and return on the solid surface assume isometric contraction of lower leg muscles. However, muscles have a finite stiffness and do lengthen by a small amount under limb tension (Biewener, 1998a; Roberts et al., 1997). Despite this difference, our estimates still hold, because in the latter case both lower leg muscles and foot tendons behave like springs, and the total stiffness remains the same (since external force and total deformation remain the same). In the case where the muscles actively shorten during stance and further lengthen the tendons (which does positive mechanical work on the tendons), the energy storage and return in the tendons would increase. However, the overall energy efficiency would decrease

(with everything else being the same), because apart from energy lost in tendon recoil, energy is further lost in the muscles that perform the mechanical work, i.e., muscle work is more expensive than tendon work (Biewener and Roberts, 2000).

In addition, the hind limb resilience obtained from anesthetized lizards was assumed to be a good estimate for hind limb resilience in running lizards. This is based on our observations that resilience was independent of torque, angular displacement, and loading rate, as well as previous findings that the damping properties of animal limbs are largely intrinsic to their structure and material properties (Weiss et al., 1988; Fung, 1993; Dudek and Full, 2006). Future studies using techniques such as tendon buckles (Biewener et al., 1998), sonomicrometry (Biewener et al., 1998), ultrasonography (Maganaris and Paul, 1999), and oxygen consumption measurement (Alexander, 2003) during locomotion are needed to confirm this assumption.

Hind foot function on granular surface: dissipative, force-generating paddle

The similarity between the observed and predicted $v_{z,CoM}$ on the granular surface supports the hypothesis of subsurface foot rotation. We speculate that on the granular surface the foot functions as a "paddle" through fluidized grains to generate force. This differs from previous observations of the utilization of solidification forces of the granular media in a legged robot (Li et al., 2009; Li et al., 2010b) and sea turtle hatchlings (Mazouchova et al., 2010) moving on granular surfaces.

As the zebra-tailed lizard's hind foot paddles through fluidized grains to generate force, energy is lost to the substrate because grain contact forces in granular media are dissipative (Nedderman, 1992). A large foot can reduce energy loss to the granular substrate compared to a small one, much like large snowshoes used by humans can reduce energy cost for walking on snow (Knapik et al., 1997). From our model of foot-ground interaction on the granular surface, for a given animal (constant weight), energy loss to the substrate is proportional to foot penetration depth, and thus inversely proportional to foot area and substrate strength (see Appendix).

Granular surface model assumptions

In our modeling of the foot-ground interaction on the granular surface using the penetration force model, we made two assumptions. First, we assumed that the ground reaction forces were insensitive to speed. This is true in the low speed regime (<0.5 m/s for our glass particles, Maladen et al., 2009) where particle inertia is negligible and forces are dominated by particle friction. Because friction is proportional to pressure, and pressure is proportional to depth (Hill et

al., 2005), granular forces in the low-speed regime are proportional to depth ($F_z=\alpha|z|A$), analogous to the hydrostatic forces in fluids ($F_z=\rho g|z|A$, i.e. buoyant forces due to hydrostatic pressure).

Second, we used the vertical stress per unit depth α determined from vertical penetration of a horizontally oriented disc to estimate forces on the foot as it rotates subsurface. In this calculation, the effective vertical stress per unit depth $\alpha\cos\theta_{foot}$ (see Appendix) depended on foot orientation via a simple relation $\cos\theta_{foot}$ (because projected area $A=A_{foot}\cos\theta_{foot}$; see Appendix), and not on direction of motion. However, our recent physics experiments (Li et al., in preparation) suggest that stresses in granular media in the low speed regime depend on both orientation and direction of motion in a more complicated manner, and that $\alpha\cos\theta_{foot}$ overestimates vertical stress per unit depth for all foot orientations and directions of motion except when the foot is horizontal and moving vertically downwards. Therefore, our model must be overestimating hydrostatic-like forces, and there must be additional forces contributing to the lizard's ground reaction forces.

We propose that these additional forces are likely from hydrodynamic-like inertial forces resulting from the local acceleration of the substrate (particles) by the foot. Analogous to hydrodynamic forces in fluids (Vogel, 1996), for an intruder moving rapidly in granular media, the particles initially at rest in front of the intruder are accelerated by, and thus exert reaction forces on, the intruder. Hydrodynamic-like forces at ~1 m/s can play an important role both in impact forces on free falling intruders (Katsuragi and Durian, 2007; Goldman and Umbanhowar, 2008) and in legged locomotion of small lightweight robots (Qian et al., 2012). We note that the foot rotation hypothesis should hold regardless, because hydrodynamic-like forces are also proportional to projected area (Katsuragi and Durian, 2007).

However, we know too little about the lizard's subsurface foot kinematics and the force laws in the high-speed regime on an intruder being pushed in a complex path within granular media (not simply a free-falling intruder) to more accurately calculate both hydrostatic-like and hydrodynamic-like forces. Future x-ray high-speed imaging experiments (Maladen et al 2009; Sharpe et al., 2012) will reveal how the lizard foot was moving subsurface. Further studies of intrusion forces in granular media in both low-speed (Li et al., 2013) and high-speed regimes can provide a more comprehensive understanding of ground reaction forces during legged locomotion on granular surfaces and provide better estimates of foot penetration depth and energy loss.

Comparison to water-running in basilisk lizard

The rapid impact of the foot on the surface at touchdown and hypothesized subsurface foot rotation appear kinematically similar to the slap and stroke phases of the basilisk lizards running on the surface of water (Glasheen and McMahon, 1996a; Hsieh, 2003). For the zebra-tailed lizard running on sand, both granular hydrostatic-like and hydrodynamic-like forces can contribute to vertical ground reaction force. This is also qualitatively similar to water-running basilisk lizard, which utilizes both hydrostatic forces resulting from the hydrostatic pressure between the water surface and the bottom of the air cavity created by the foot, and hydrodynamic forces resulting from the water being accelerated from rest by the rapidly moving foot (Glasheen and McMahon, 1996a, 1996b; Hsieh and Lauder, 2004).

However, the degree to which each species relies on these two categories of forces differs due to differences in the properties of the supporting media. For given foot size, depth, and speed, the hydrostatic(-like) forces in water are an order of magnitude smaller than the hydrostatic-like forces in granular media, whereas the hydrodynamic(-like) forces are similar between in water and in granular media (see Appendix). As a result, the basilisk lizard running on water must rely on hydrodynamic forces to a larger degree than the zebra-tailed lizard running on sand, considering that these two lizards have similar size (~ 0.1 m). An extreme example for this is that it is impossible for a basilisk lizard to stand on the surface of water, but a zebra-tailed lizard can stand on loose sand.

Motor function of upper hind leg

Despite the passive nature of the leg spring in the spring-mass model, animal limbs do not function purely passively as springs—the muscles within them must perform mechanical work. We have shown that on the solid surface, the lizard's hind foot saves about 40% of the mechanical work per step. The remaining 60% is lost either within the foot or to the ground, and must be compensated by mechanical work performed by muscles, which is $W_{muscle} = 0.11 \pm 0.10$. This work is likely provided by knee extension during the second half of stance (Fig. 6D, red curve) powered by the upper leg muscles.

On the granular surface, substantial energy is lost to the substrate. This is in accord with previous observations of higher mechanical energetic cost during locomotion on granular surfaces in human (Zamparo et al., 1992; Lejeune et al., 1998) and legged robots (Li et al., 2010a). Because the energy lost to the substrate equals the reduction in CoM mechanical energy during the first half of stance, even without energy loss within the limb, the upper hind leg muscles must perform mechanical work of $W_{muscle} = 0.31 \pm 0.10$ during the second half of stance, about three times that

on the solid surface for a given animal running at a given speed, as evidenced by the larger knee extension on the granular surface (Fig. 6D, blue curve).

Our models of the foot-ground interaction on both surfaces assume purely passive foot mechanics, and do not consider the role of active neurosensory control. However, animals can actively adjust kinematics and muscle function to accommodate changes in surface conditions (Ferris et al., 1999; Daley and Biewener, 2006). We observed that when confronted by a substrate which transitioned from solid into granular (or *vice versa*), the lizard displayed partial adjustment of foot posture during the first step on the new surface, followed by full adjustment during the second step. Future studies using neuromechanics techniques, such as EMG (Biewener et al., 1998; Sponberg and Full, 2008; Sharpe and Goldman, in review) and denervation and reinnervation (Chang et al., 2009), can determine how neural control and sensory feedback mechanisms are used to control limb function to accommodate changing substrates.

Conclusions

During running on both solid and granular surfaces, the zebra-tailed lizard displayed spring-mass-like center of mass kinematics with distinct hind foot, hind leg, and trunk kinematics. The lizard's large, elongate hind foot served multiple functions during locomotion. On the solid surface, the hind foot functioned as an energy-saving spring and reduced about 40% of the mechanical work needed each footstep. On the granular surface, the hind foot paddled through fluidized grains to generate force, and substantial energy was lost during irreversible deformation of the granular substrate. The energy lost within the foot and to the substrate must be compensated for by mechanical work done by the upper hind leg muscles.

The multifunctional hind foot may passively (and possibly actively) adjust to the substrate during locomotion in natural terrain, and provide this desert generalist with energetic advantages and simplify its neurosensory control tasks (Full and Koditschek, 1999). Current robotic devices often suffer performance loss and high cost of transport on flowing substrates like granular material (Kumagai 2004; Li et al., 2009; Li et al., 2010b; Li et al., 2010a). Insights from studies like ours can provide inspiration for next-generation multi-terrain robots (Pfeifer et al., 2007). Finally, our study also highlights the need for comprehensive force models for granular media (Li et al., in preparation) and for flowing terrestrial environments in general.

Appendix

Small relative oscillation in forward speed

Running at 1.1 m/s, the lizard's Froude number in the sagittal plane was $Fr = v_{x,CoM}^2/gL_0 = 3$ (where $L_0 \approx 4$ cm is the leg length at touchdown), above the typical value of 2.5 where most animals transition from trotting to galloping (Alexander, 2003). This implied that the kinetic energy ($\frac{1}{2} mv_{CoM}^2 \approx \frac{1}{2} mv_{x,CoM}^2$) of the CoM was 3 times larger than its gravitational potential energy (mgz_{CoM}). Because both the forward speed oscillation $\Delta v_{x,CoM}$ and vertical speed oscillation $\Delta v_{z,CoM}$ were determined by the total ground reaction force and the attack angle of the leg spring ($\beta = \sin^{-1}(v_{x,CoM}DT/2L_0) = 0.9$ rad), they must be of the same order of magnitude (Blickhan, 1989), i.e., $\Delta v_{x,CoM} \sim \Delta v_{z,CoM}$. From the observed CoM kinematics, $\Delta v_{z,CoM} < (gL_0)^{1/2}$. Therefore, $\Delta v_{x,CoM} \sim \Delta v_{z,CoM} < (gL_0)^{1/2} << v_{x,CoM}$, and $\Delta v_{x,CoM}/v_{x,CoM} << 1$.

Hind foot curvature on solid surface

Three-dimensional kinematics showed that the hind limb (from the hip to the digit tip of the fourth toe) remained nearly within a plane during the entire stride (out-of-plane component is 5% averaged over the entire stride). During stance, the orientation of the foot plane remained nearly unchanged, with a foot sprawl angle of 53 ± 4° relative to the sagittal plane in the posterior view. Hind foot curvature κ could then be obtained by fitting a circle to the hind foot (from the ankle to the digit tip) within the foot plane and determining the radius of curvature ρ of the fit circle (see diagram in Fig. 9A), i.e., $\kappa = \pm 1/\rho$, where + sign indicates foot hyperextension, – sign indicates foot flexion, and $\kappa = 0$ indicates a straight foot.

Tendon spring deformation

From the two-dimensional strut-spring model of the hind limb, by geometry, the tendon spring deformation Δl was related to the observed changes of joint angles and the foot joint radii as: $\Delta l = \Sigma_i r_i \Delta\theta_i$, where i = K, A, MP, PP were the four joints in the model, $\Delta\theta_i$ the observed changes of joint angles, and r_i the joint radii ($r_K = r_A = 1.25$ mm, $r_{MP} = 0.75$ mm, $r_{PP} = 0.50$ mm). We observed that the relaxed hind foot of a live animal was nearly straight (Fig. 1A), which was similar to the foot shape at touchdown during running (Fig. 3A,E). Thus we defined the relaxed length of the tendon spring as the length when the foot was straight, i.e., $\Delta l = 0$ at touchdown. Calculated maximal tendon spring deformation $\Delta l_{max} = 0.78$ mm corresponded to a 3% strain. We did not consider tendon spring deformation in the swing phase (dotted curve in Fig. 6F) because the assumption of isometric contraction of lower leg muscles was only valid for the stance phase.

Tendon spring stiffness

The stiffness of the tendon spring was defined as the maximal tension divided by the maximal deformation of the tendon spring, i.e., $k = T_{max}/\Delta l_{max}$. From the observed CoM kinematics, the total ground reaction force at mid-stance was F_{max} = 0.3 N within the coronal plane and pointed from the digit tip to the hip. At mid-stance, because the foot was neither dorsiflexing nor plantarflexing, torque was balanced at the ankle, i.e., $T_{max}r_A = F_{max}\Delta x_{AT}$, where Δx_{AT} = 1.4 cm was the horizontal distance between the ankle and the digit tip at mid-stance, and r_A = 1.25 mm. Thus T_{max} = 3.4 N and $k = 4.4 \times 10^3$ N/m. The maximal stress in the foot tendons during stance was $\sigma_{max} = T_{max}/\pi r_{PP}^2$ = 4.3 MPa.

The torsional stiffness of the ankle observed in anesthetized lizards from the modified work loop experiments ($\sim 1 \times 10^{-3}$ Nm/rad) was an order of magnitude smaller than estimated from running kinematics (12×10^{-3} Nm/rad). This is however not contradictory but expected because during stance the lizard's lower leg muscles must be activated, and the resulting higher tension from muscle contraction increases limb stiffness (Weiss et al., 1988).

Foot elongation increases energy savings on solid surface

The stiffness of a piece of elastic material like a tendon is $k = E_0A_0/l_0$, where E_0 is the Young's modulus, A_0 the cross sectional area, and l_0 the rest length of the material. Most animal tendons are primarily made of collagen (Kirkendall and Garrett, 1997) and are of similar Young's modulus (i.e., E_0 is nearly constant). Thus, the stiffness of the tendon spring scales as $k \propto A_0/l_0 \propto r_0^2/l_0$, i.e., an elongate tendon (smaller r_0 and larger l_0) is less stiff and stretches more easily than a short, thick tendon. Because elastic energy storage decreases with tendon stiffness ($E_{storage} = \frac{1}{2} k\Delta l_{max}^2 = \frac{1}{2} T_{max}^2/k \propto 1/k$ for a given T_{max}), an elongate tendon can store (and return) more energy.

An elongate foot also reduces the moment arm of tendon tension (small r_A) but increases the moment arm of the ground reaction force (large Δx_{AT}) about the ankle, therefore reducing the mechanical advantage (Biewener et al., 2004), so it increases tension in the foot for a given ground reaction force (because $T_{max} = F_{max}\Delta x_{AT}/r_A$) and amplifies tendon stretch for enhanced energy storage and return.

Vertical ground reaction force on granular surface

We assumed that the hind foot was rotating at a constant angular velocity ω about the moving ankle during stance, i.e., $\theta_{foot} = \omega t$ within $0 \le t \le DT$ and $0 \le \theta_{foot} \le \pi/2$, then $\omega = \pi/2DT = 10\pi/9T$

= 35 rad/s. From the measured vertical speed of the ankle and this assumed foot rotation, the vertical speed of most (75%) of the foot was always below 0.5 m/s during most (75%) of stance.

Given foot rotation $\theta_{foot} = \omega t$, the foot area projected in the horizontal plane decreased with time as $A = A_{foot}\cos\omega t$, where A_{foot} = 1 cm^2 is the hind foot area; the foot depth (measured at the center of the foot) increased with time as $|z| = |z|_{max}\sin\omega t$. The vertical ground reaction force on the foot was then sinusoidal: $F_z = F_{z,max}\sin 2\omega t$, which was sinusoidal, where $F_{z,max} = \alpha A_{foot}|z|_{max}\sin\pi/4\cos\pi/4 = \frac{1}{2}\alpha A_{foot}|z|_{max}$. For steady state locomotion on a level surface, the F_z generated by one foot averaged over a cycle must equal half the body weight, i.e., $\int_0^T F_{z,max} sin2\omega t\, dt = \frac{1}{2}mg$. Therefore, $F_{z,max} = 5\pi mg/9$ and $F_z = 5\pi mg/9 \sin 10\pi t/9T$.

Energy loss to granular substrate

By integration of vertical ground reaction force over vertical displacement of the foot, the energy loss to the granular substrate was $E_{substrate} = \int_0^{|z|_{max}} F_z\, d|z| = \int_0^T F_z \frac{d|z|}{dt} dt$, where $|z|_{max}$ = 1.0 cm from $F_{z,max} = \frac{1}{2}\alpha A_{foot}|z|_{max}$. The hypothesized foot rotation in the sagittal plane did not take into account the sprawl of the foot during stance, which could induce additional energy loss by lateral displacement of the granular substrate. However, a sprawled foot posture did not affect the condition of vertical force balance and thus did not change our estimate of energy dissipation in the sagittal plane. Therefore this estimate provides a lower bound.

Large foot area reduces energy loss on granular surface

For a given animal (constant weight mg), $F_{z,max} = \frac{1}{2}\alpha A_{foot}|z|_{max} = 5\pi mg/9$ is constant, thus $E_{substrate} = |z|_{max} \int_0^T F_z\ \omega\, cos\omega t\, dt \propto |z|_{max} \propto 1/(\alpha A_{foot})$. This implies that the energy loss to the granular substrate increases with foot penetration depth. On a given granular surface (fixed α), a larger foot (larger A_{foot}) sinks less than a smaller foot, and thus loses less energy to the substrate. For a given foot size (fixed A_{foot}), a foot sinks less on a stronger granular substrate (larger α) than on a weaker substrate, and thus loses less energy to the substrate.

Comparison of forces in granular media and in water

For water, hydrostatic force is $F_z = \rho g|z|A$. Comparing this with $F_z = \alpha|z|A$ for granular media, ρg is the equivalent of α. For water, $\rho g = 1.0 \times 10^4$ N/m^3; for loosely packed glass particles, $\alpha = 3.5 \times 10^5$ N/m^3. Therefore, the hydrostatic forces in water are an order of magnitude smaller than the hydrostatic-like forces in granular media for given foot size and depth.

Hydrodynamic(-like) forces should be proportional to the density of the surrounding media because they are due to the media being accelerated. For water, $\rho = 1.0 \times 10^3$ N/m^3; for loosely packed glass particles the effective density is 2.5×10^3 N/m^3 × 0.58 volume fraction = 1.45×10^3 N/m^3. Therefore, the hydrodynamic forces in water and hydrodynamic-like forces in granular media are on the same order of magnitude for given foot size and foot speed.

Acknowledgements

We gratefully thank Sarah Sharpe, Yang Ding, Nick Gravish, Ryan Maladen, Paul Umbanhowar, Kyle Mara, Young-Hui Chang, Andy Biewener, Tom Roberts, Craig McGowan, and two anonymous reviewers for helpful discussions and/or comments on the manuscript; Loretta Lau for help with kinematics data tracking; Sarah Sharpe for help with animal protocol and anesthetization; Mateo Garcia, Nick Gravish, and Andrei Savu for help with force plate setup; Ryan Maladen and The Sweeney Granite Mountains Desert Research Center for help with animal collection; and the staff of The Physiological Research Laboratory animal facility of The Georgia Institute of Technology for animal housing and care. This work was funded by The Burroughs Wellcome Fund (D.I.G. and C.L.), The Army Research Laboratory Micro Autonomous Systems and Technology Collaborative Technology Alliance (D.I.G. and C.L.), The Army Research Office Biological Locomotion Principles and Rheological Interaction Physics (D.I.G. and C.L.) and The University of Florida and Temple University start-up funds (S.T.H.).

References

Alexander, R. M. (2003). *Principles of Animal Locomotion*. Princeton: Princeton University Press.

Alexander, R. M. and Vernon, A. (1975). The mechanics of hopping by kangaroos (*Macropodidae*). *Journal of Zoology* **177**, 265–303.

Autumn, K., Liang, Y. A., Hsieh, S. T., Zesch, W., Chan, W. P., Kenny, T. W., Fearing, R. S. and Full, R. J. (2000). Adhesive force of a single gecko foot-hair. *Nature* **405**, 681–685.

Bauwens, D., Garland Jr., T., Castilla, A. M. and Van Damme, R. (1995). Evolution of sprint speed in lacertid lizards: morphological, physiological and behavioral covariation. *Evolution* **49**, 848–863.

Biewener, A. A. (1998a). Muscle function in vivo: A comparison of muscles used for elastic energy savings versus muscles used to generate mechanical power. *Integrative & Comparative Biology* **38**, 703–717.

Biewener, A. A. (1998b). Muscle-tendon stresses and elastic energy storage during locomotion in the horse. *Comparative Biochemistry and Physiology Part B: Biochemistry & Molecular Biology* **120**, 73–87.

Biewener, A. A., Alexander, R. M. and Heglund, N. C. (1981). Elastic energy storage in the hopping of kangaroo rats (*Dipodomys spectabilis*). *Journal of Zoology* **195**, 369–383.

Biewener, A. A. and Blickhan, R. (1988). Kangaroo rat locomotion: design for elastic energy storage or acceleration? *The Journal of Experimental Biology* **140**, 243–255.

Biewener, A. A., Farley, C. T., Roberts, T. J. and Temaner, M. (2004)**.** Muscle mechanical advantage of human walking and running: implications for energy cost. *Journal of Applied Physiology* **97**, 2266–2274.

Biewener, A. A., Konieczynski, D. D. and Baudinette, R. V. (1998). In vivo muscle force-length behavior during steady-speed hopping in tammar wallabies. *The Journal of Experimental Biology* **201**, 1681–1694.

Biewener, A. A. and Roberts, T. J. (2000). Muscle and tendon contributions to force, work, and elastic energy savings: a comparative perspective. *Exercise and Sport Sciences Reviews* **28**, 99–107.

Blickhan, R. (1989). The spring-mass model for running and hopping. *Journal of Biomechanics* **22**, 1217–1227.

Blickhan, R. and Full R. J. (1993). Similarity in multilegged locomotion: Bouncing like a monopode. *Journal of Comparative Physiology* **173**, 509–517.

Chang, Y.-H., Auyang, A. G., Scholz, J. P. and Nichols, T. R. (2009). Whole limb kinematics are preferentially conserved over individual joint kinematics after peripheral nerve injury. *The Journal of Experimental Biology* **212**, 3511–3521.

765 **Chen, J. J., Peattie, A. M., Autumn, K. and Full, R. J.** (2006). Differential leg function in a
766 sprawled-posture quadrupedal trotter. *The Journal of Experimental Biology* **209**, 249–259.

767 **Coombs Jr., W. P.** (1978). Theoretical aspects of cursorial adaptations in dinosaurs. *The*
768 *Quarterly Review of Biology* **53**, 393–418.

769 **Crawford, C. S.** (1981). *Biology of Desert Invertebrates.* New York: Springer.

770 **Daley, M. A. and Biewener, A. A.** (2006). Running over rough terrain reveals limb control for
771 intrinsic stability. *Proceedings of the National Academy of Sciences of the United States of*
772 *America* **103**, 15681–15686.

773 **Dickinson, M. H., Farley, C. T., Full, R. J., Koehl, M. A. R., Kram, R. and Lehman, S.**
774 (2000). How animals move: An integrative view. *Science* **288**, 100–106.

775 **Dickinson, W. W. and Ward, J. D.** (1994). Low depositional porosity in eolian sands and
776 sandstones, Namib Desert. *Journal of Sedimentary Research* **64**, 226–232.

777 **Ding, Y., Gravish, N. and Goldman, D. I.** (2011a). Drag induced lift in granular media.
778 *Physical Review Letters* **106**, 028001(1–4).

779 **Dudek, D. M. and Full, R. J.** (2006). Passive mechanical properties of legs from running insects.
780 *The Journal of Experimental Biology* **209**, 1502–1515.

781 **Farley, C. T. and Ko, T. C.** (1997). Mechanics of locomotion in lizards. *The Journal of*
782 *Experimental Biology* **200**, 2177–2188.

783 **Ferris, D., Liang, K. and Farley, C. T.** (1999). Runners adjust leg stiffness for their first step on
784 a new running surface. *Journal of Biomechanics* **32**, 787–794.

785 **Ferris, D. P., Louie, M. and Farley, C. T.** (1998). Running in the real world: Adjusting leg
786 stiffness for different surfaces. *Proceedings of the Royal Society B: Biological Sciences* **265**, 989–
787 994.

788 **Full, R. J. and Koditschek, D. E.** (1999). Templates and anchors: neuromechanical hypotheses
789 of legged locomotion on land. *The Journal of Experimental Biology* **202**, 3325–3332.

790 **Fung, Y. C.** (1993). *Biomechanics: Mechanical Properties of Living Tissues*. New York:
791 Springer.

Garland Jr., T. and Janis, C. (1993). Does metatarsal/femur ratio predict maximal running speed in cursorial mammals? *Journal of Zoology* **229**, 133–151.

Glasheen, J. W. and McMahon, T. A. (1996a). A hydrodynamic model of locomotion in the Basilisk Lizard. *Nature* **380**, 340–341.

Glasheen, J. W. and McMahon, T. A. (1996b). Vertical water entry of disks at low Froude numbers. *Physics of Fluids* **8**, 2078–2083.

Goldman, D. I. and Umbanhowar, P. B. (2008). Scaling and dynamics of sphere and disk impact into granular media. *Physical Review E* **77**, 021308(1–14).

Gravish, N., Umbanhowar, P. B. and Goldman, D. I. (2010). Force and flow transition in plowed granular media. *Physical Review Letters* **105**, 208301(1–4).

Hedrick, T. L. (2008). Software techniques for two- and three-dimensional kinematic measurements of biological and biomimetic systems. *Bioinspiration & Biomimetics* **3**, 034001(1–6).

Hill, G., Yeung, S. and Koehler, S. A. (2005). Scaling vertical drag forces in granular media. *Europhysics Letters* **72**, 137–143.

Holmes, P., Full, R. J., Koditschek, D. and Guckenheimer, J. (2006). The dynamics of legged locomotion: Models, analyses, and challenges. *SIAM Review* **48**, 207–304.

Hsieh, S. T. (2003). Three-dimensional hindlimb kinematics of water running in the plumed basilisk lizard (*Basiliscus plumifrons*). *The Journal of Experimental Biology* **206**, 4363–4377.

Hsieh, S. T. and Lauder, G. V. (2004). Running on water: Three-dimensional force generation by basilisk lizards. *Proceedings of the National Academy of Sciences of the United States of America* **101**, 16784–16788.

Irschick, D. J. and Jayne, B. C. (1999a). Comparative three-dimensional kinematics of the hindlimb for high speed bipedal and quadrupedal locomotion of lizards. *The Journal of Experimental Biology* **202**, 1047–1065.

Irschick, D. J. and Jayne, B. C. (1999b). A field study of the effects of incline on the escape locomotion of a bipedal lizard, *Callisaurus draconoides*. *Physiological and Biochemical Zoology* **72**, 44–56.

Jindrich, D. L. and Full, R. J. (1999). Many-legged maneuverability: dynamics of turning in hexapods. *The Journal of Experimental Biology* **202**, 1603–1623.

Karasov, W. H. and Anderson, R. A. (1998). Correlates of average daily metabolism of field-active zebra-tailed lizards (*Callisaurus draconoides*). *Physiological Zoology* **71**, 93–105.

Katsuragi, H. and Durian, D. J. (2007). Unified force law for granular impact cratering. *Nature Physics* **3**, 420–423.

Ker, R. F., Bennett, M. B., Bibby, S. R., Kester, R. C. and Alexander, R. M. (1987). The spring in the arch of the human foot. *Nature* **325**, 147–149.

Kirkendall, D. T. and Garrett, W. E. (1997). Function and biomechanics of tendons. *Scandinavian Journal of Medicine & Science in Sports* **7**, 62–66.

Knapik, J., Hickey, C., Ortega, S., Nagel, J. and De Pontbriand, R. (2002). Energy cost during locomotion across snow: a comparison of four types of snowshoes with showshoe design considerations. *Work* **18**, 171–177.

Korff, W. L. and McHenry, M. J. (2011). Environmental differences in substrate mechanics do not affect sprinting performance in sand lizards (*Uma scoparia* and *Callisaurus draconoides*). *The Journal of Experimental Biology* **214**, 122–130.

Kumagai, J. (2004). Sand trip—DARPA's 320-kilometer robotic race across the Mojave Desert yields no winner, but plenty of new ideas. *IEEE Spectrum* **41**, 44–50.

Lejeune, T. M., Willems, P. A. and Heglund, N. C. (1998). Mechanics and energetics of human locomotion on sand. *The Journal of Experimental Biology* **201**, 2071–2080.

Li, C., Hoover, A. M., Birkmeyer, P., Umbanhowar, P. B., Fearing, R. S. and Goldman, D. I. (2010a). Systematic study of the performance of small robots on controlled laboratory substrates. *Proceedings of SPIE* **7679**, 76790Z(1–13).

Li, C., Umbanhowar, P. B., Komsuoglu, H. and Goldman, D. I. (2010b). The effect of limb kinematics on the speed of a legged robot on granular media. *Experimental Mechanics* **50**, 1383–1393.

Li, C., Umbanhowar, P. B., Komsuoglu, H., Koditschek, D. E. and Goldman, D. I. (2009). Sensitive dependence of the motion of a legged robot on granular media. *Proceedings of the National Academy of Sciences of the United States of America* **106**, 3029–3034.

Li, C., Zhang, T. and Goldman, D. I. (2013). A terradynamics of legged locomotion on granular media. *Science*, **339**, 1408–1411.

Maganaris, C. N. and Paul, J. P. (1999). In vivo human tendon mechanical properties. *Journal of Physiology* **521**, 307–313.

Maladen, R. D., Ding, Y., Li, C. and Goldman, D. I. (2009). Undulatory swimming in sand: Subsurface locomotion of the sandfish lizard. *Science* **325**, 314–318.

Maladen, R. D., Ding, Y., Umbanhowar, P. B., Kamor, A. and Goldman, D. I. (2011). Mechanical models of sandfish locomotion reveal principles of high performance subsurface sand-swimming. *Journal of The Royal Society Interface* **8**, 1332-1345.

Matson J. (2010). Unfree Spirit: NASA's Mars rover appears stuck for good. *Scientific American*, **302**, 16.

Mazouchova, N., Gravish, N., Savu, A. and Goldman, D. I. (2010). Utilization of granular solidification during terrestrial locomotion of hatchling sea turtles. *Biology letters* **6**, 398–401.

McGowan, C. P., Skinner, J. and Biewener, A. A. (2008). Hind limb scaling of kangaroos and wallabies (superfamily *Macropodoidea*): Implications for hopping performance, safety factor and elastic savings. *Journal of Anatomy* **212**, 153–163.

Moritz, C. T. and Farley, C. T. (2003). Human hopping on damped surfaces: Strategies for adjusting leg mechanics. *Proceedings of the Royal Society B: Biological Sciences* **270**, 1741–1746.

Mosauer, W. (1932). Adaptive convergence in the sand reptiles of the Sahara and of California: A study in structure and behavior. *Copeia* **1932**, 72–78.

Nedderman, R. M. (1992). *Statics and Kinematics of Granular Materials*. Cambridge: Cambridge University Press.

Pfeifer, R., Lungarella, M. and Iida, F. (2007). Self-organization, embodiment, and biologically inspired robotics. *Science* **318**, 1088–1093.

Qian F., Zhang T., Li C., Masarati, P., Hoover A.M., Birkmeyer P., Pullin A., Fearing R.S. and Goldman D.I. (2012). Walking and running on yielding and fluidizing ground. *Robotics: Science and Systems* (in press).

Roberts, T. J., Marsh, R. L., Weyand, P. G. and Taylor, C. R. (1997). Muscular force in running turkeys: The economy of minimizing work. *Science* **275**, 1113–1115.

Rubenson, J., Lloyd, D. G., Heliams, D. B., Besier, T. F. and Fournier, P. A. (2011). Adaptations for economical bipedal running: The effect of limb structure on three-dimensional joint mechanics. *Journal of The Royal Society Interface* **8**, 740–755.

Russell, A. P. (1993). The aponeuroses of the lacertilian ankle. *Journal of Morphology* **218**, 65–84.

Schmitt, J., Garcia, M., Razo, R. C., Holmes, P. and Full, R. J. (2002). Dynamics and stability of legged locomotion in the horizontal plane: A test case using insects. *Biological Cybernetics* **86**, 343–353.

Sharpe, S. S., Ding, Y., and Goldman, D. I. (2012). Environmental interaction influences muscle activation strategy during sand-swimming in the sandfish lizard (*Scincus scincus*). *The Journal of Experimental Biology* **216**, 260–274.

Spagna, J. C., Goldman, D. I., Lin, P.-C., Koditschek, D. E. and Full, R. J. (2007). Distributed mechanical feedback in arthropods and robots simplifies control of rapid running on challenging terrain. *Bioinspiration & Biomimetics* **2**, 9–18.

Spence, A. J., Revzen, S., Seipel, J., Mullens, C. and Full, R. J. (2010). Insects running on elastic surfaces. *The Journal of Experimental Biology* **213**, 1907–1920.

Sponberg, S. and Full, R. J. (2008). Neuromechanical response of musculo-skeletal structures in cockroaches during rapid running on rough terrain. *The Journal of Experimental Biology* **211**, 433–446.

Vitt, L. J. and Ohmart, R. D. (1977). Ecology and reproduction of lower Colorado River lizards: I. *Callisaurus draconoides* (*Iguanidae*). *Herpetologica* **33**, 214–222.

Vogel, S. (1996). *Life in Moving Fluids: The Physical Biology of Flow*. Princeton: Princeton University Press.

Weiss, P. L., Hunter, I. W. and Kearney, R. E. (1988). Human ankle joint stiffness over the full range of muscle activation levels. *Journal of Biomechanics* **21**, 539–544.

Zamparo, P., Perini, R., Orizio, C., Sacher, M. and Ferretti, G. (1992). The energy cost of walking or running on sand. *European Journal of Applied Physiology and Occupational Physiology* **65**, 183–187.

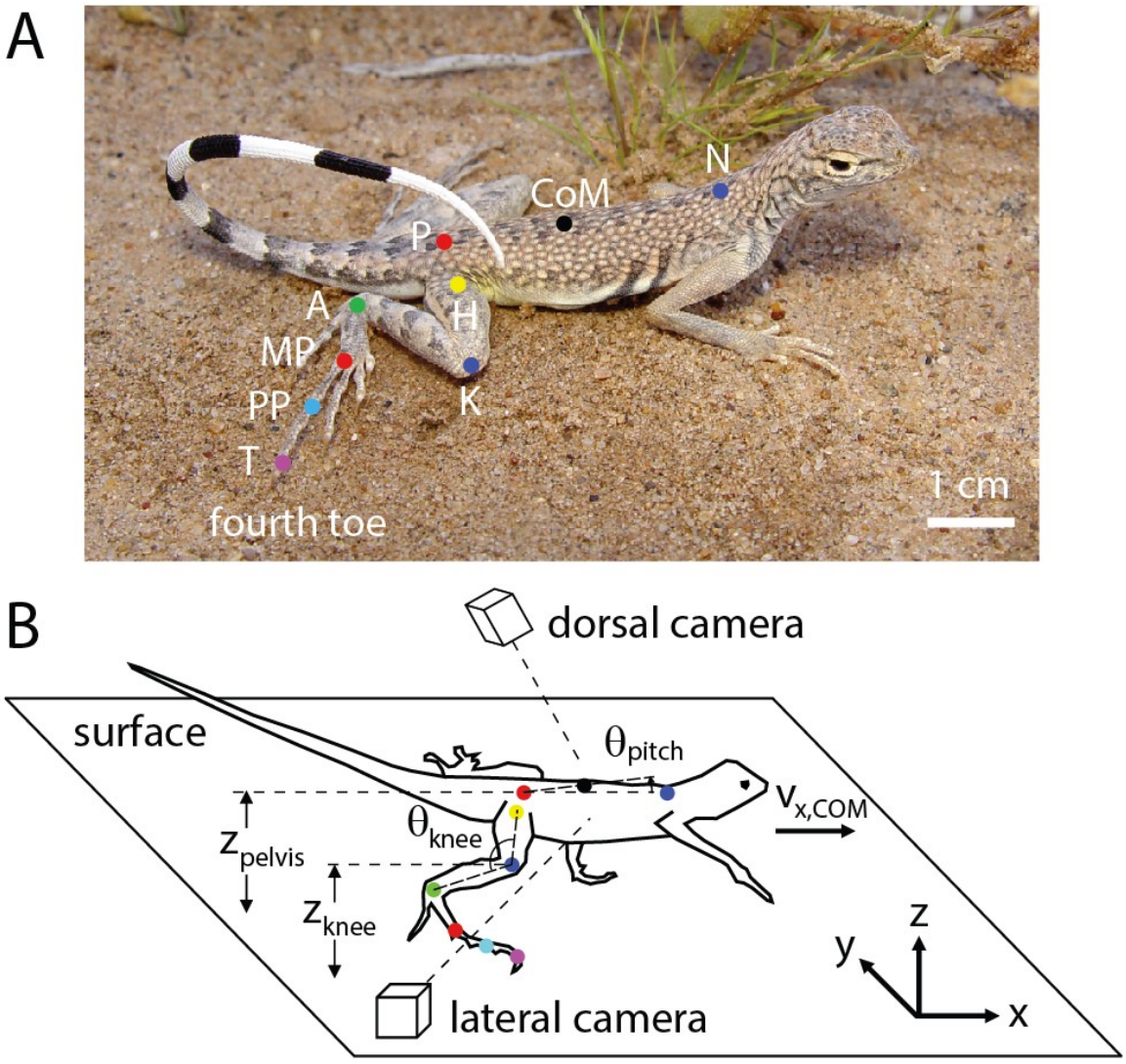

909

910 Fig. 1. Model organism and three-dimensional kinematics experiments. (A) A zebra-tailed lizard
911 resting on sand in the wild (photo: Thomas C. Brennan). (B) Experimental setup for three-
912 dimensional kinematics capture, with definitions of pelvis height (z_{pelvis}), knee height (z_{knee}), trunk
913 pitch angle (θ_{pitch}), and knee angle (θ_{knee}). Colored dots in (A,B) are digitized points on the
914 midline of the trunk, hind leg, and elongate hind foot.

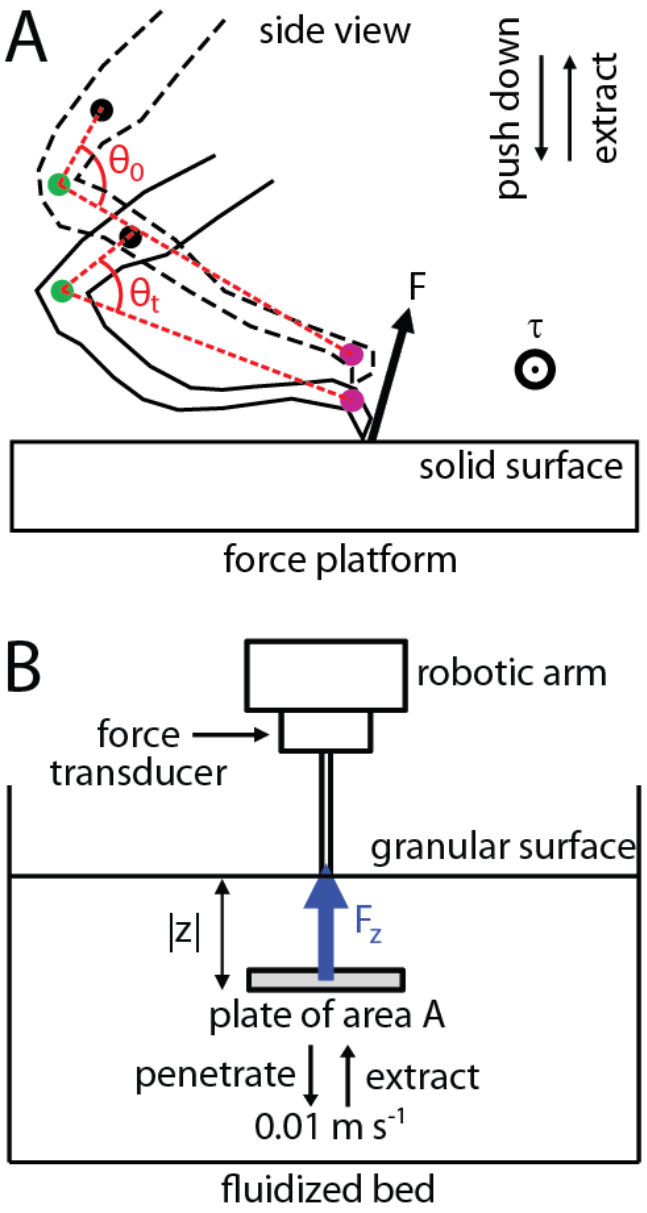

915

916 Fig. 2. Experiments to measure hind limb resilience and granular penetration force. (A)
917 Experimental setup for hind limb resilience measurements. Dashed foot tracing shows the relaxed,
918 straight foot right before touchdown. Solid foot tracing shows the hyperextended foot during
919 ground contact. *F*, ground reaction force; θ_0, angle between the ankle and the digit tip in the
920 relaxed, straight foot; θ_t, angle between the ankle and the digit tip in the hyperextended foot; τ,
921 torque about the ankle. (B) Experimental setup for granular penetration force measurements.

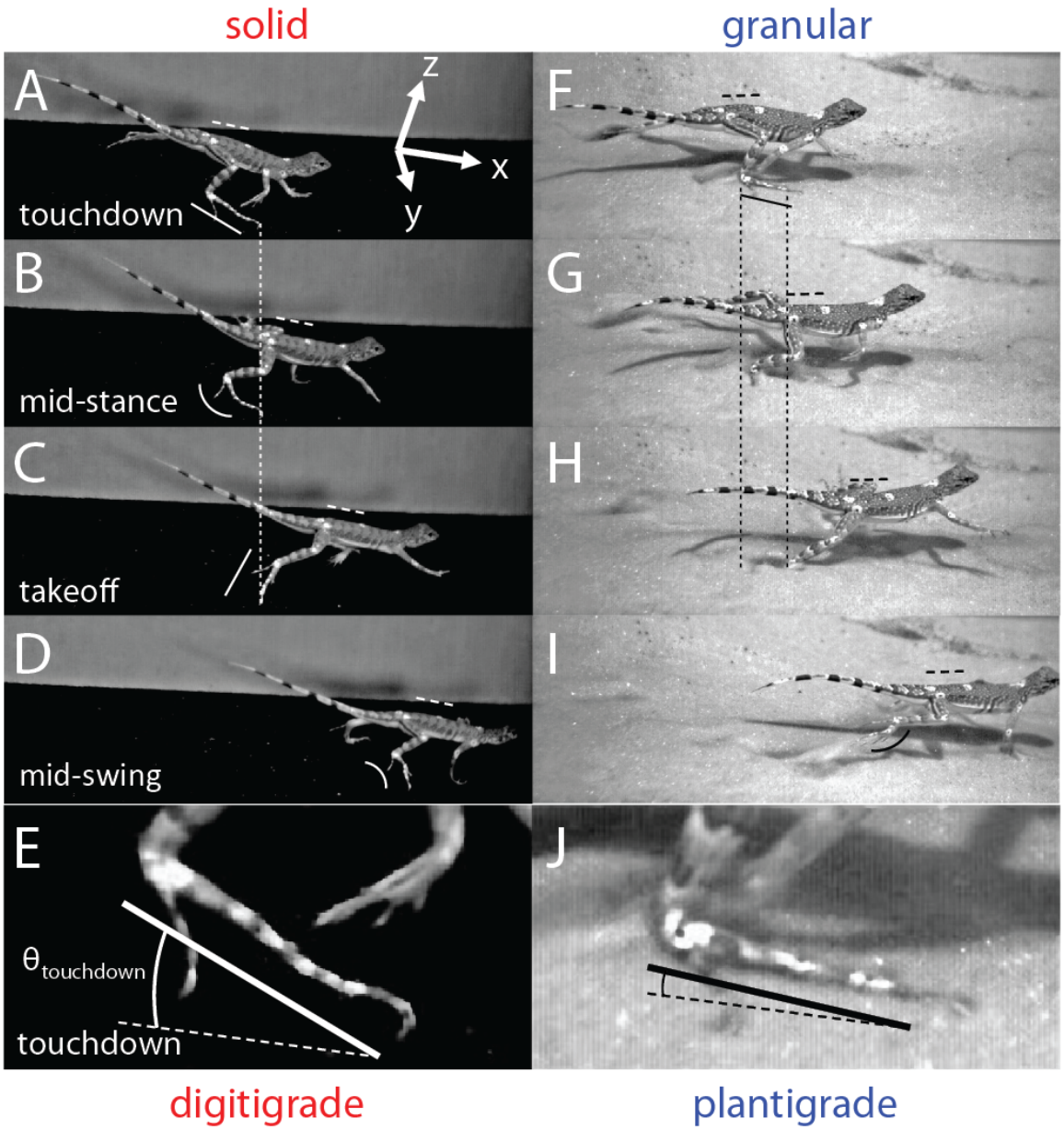

922

923 Fig. 3. Lateral views of representative runs on the solid (A–D) and the granular (F–I) surface (see
924 Movies 1, 2 in supplementary material). (E,J) Closer views of foot posture at touchdown showing
925 definition of touchdown foot angle $\theta_{touchdown}$. Solid lines and curves along the foot indicate hind
926 foot posture and shape. Note that the lateral camera was oriented at an angle to the *x*, *y*, *z* axes
927 such that forward (+*x*) direction appeared to point slightly downwards.

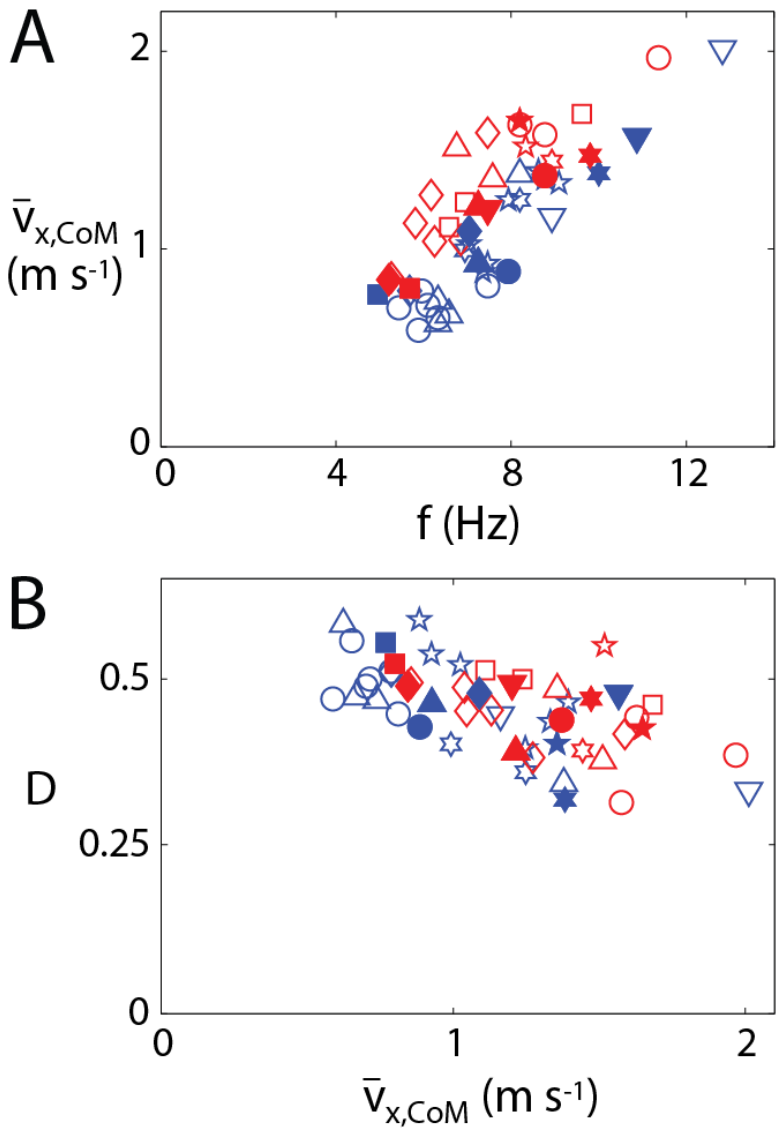

928

929 Fig. 4. Performance and gait on the solid (red) and the granular (blue) surfaces. (A) Average
930 forward speed vs. stride frequency. (B) Duty factor vs. average forward speed. Different symbols
931 represent different individuals. Filled symbols are from the seven representative runs for each of
932 the seven individuals tested on both substrates. Empty symbols are from runs that were not
933 included in the representative data set.

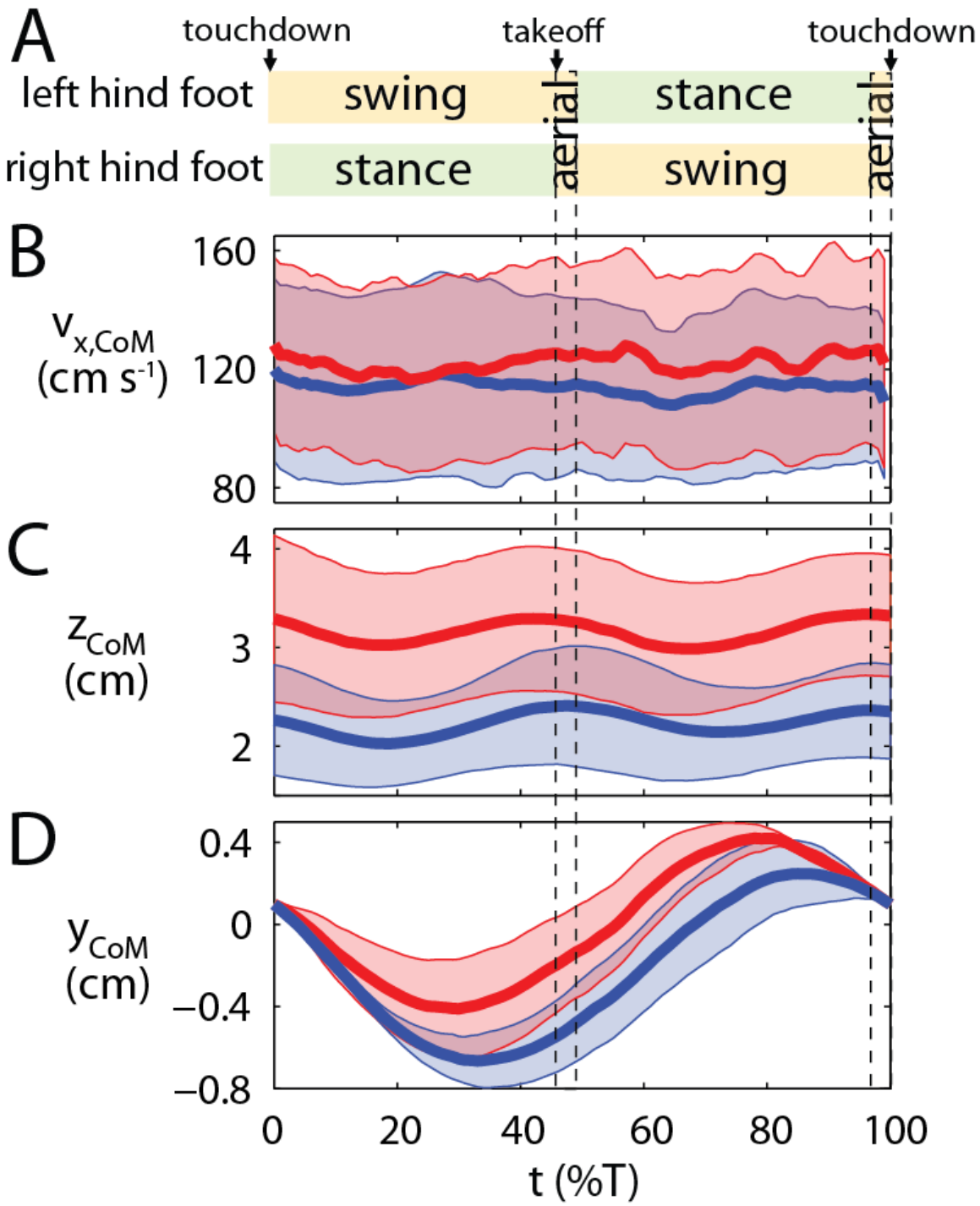

934

935 Fig. 5. Center of mass (CoM) kinematics (mean ± s.d.) vs. time during a stride on the solid (red)
936 and the granular (blue) surfaces. (A) Footstep pattern. (B) CoM forward speed. (C) CoM vertical
937 position. (D) CoM lateral position. See Fig. 1 for definitions of kinematic variables.

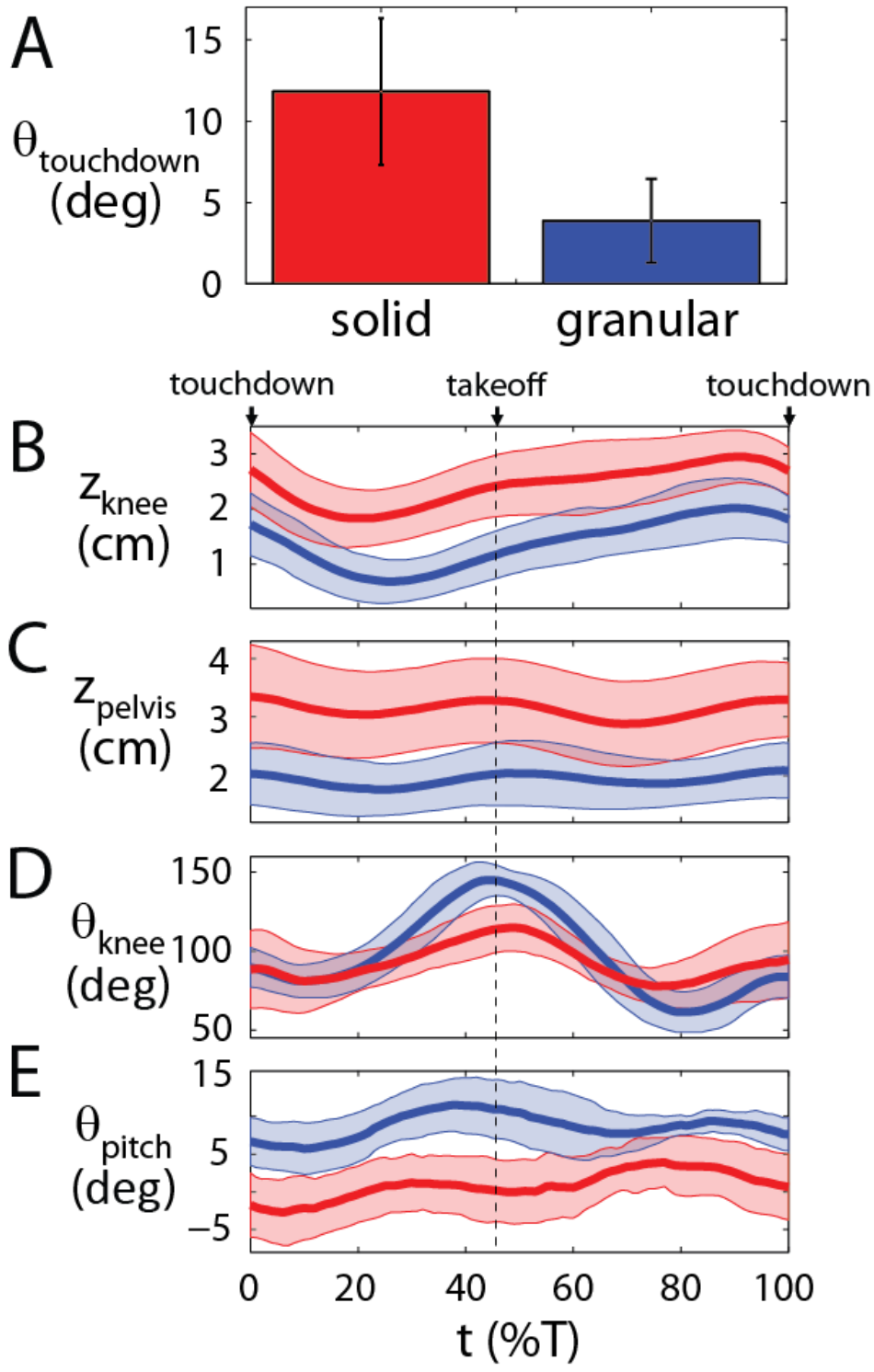

938

939 Fig. 6. Hind foot, hind leg, and trunk kinematics (mean ± s.d.) vs. time during a stride on the solid
940 (red) and the granular (blue) surfaces. (A) Touchdown foot angle. (B) Knee height. (C) Pelvis
941 height. (D) Knee angle. (E) Trunk pitch angle. See Fig. 1 and Fig. 3E,J for definitions of
942 kinematic variables.

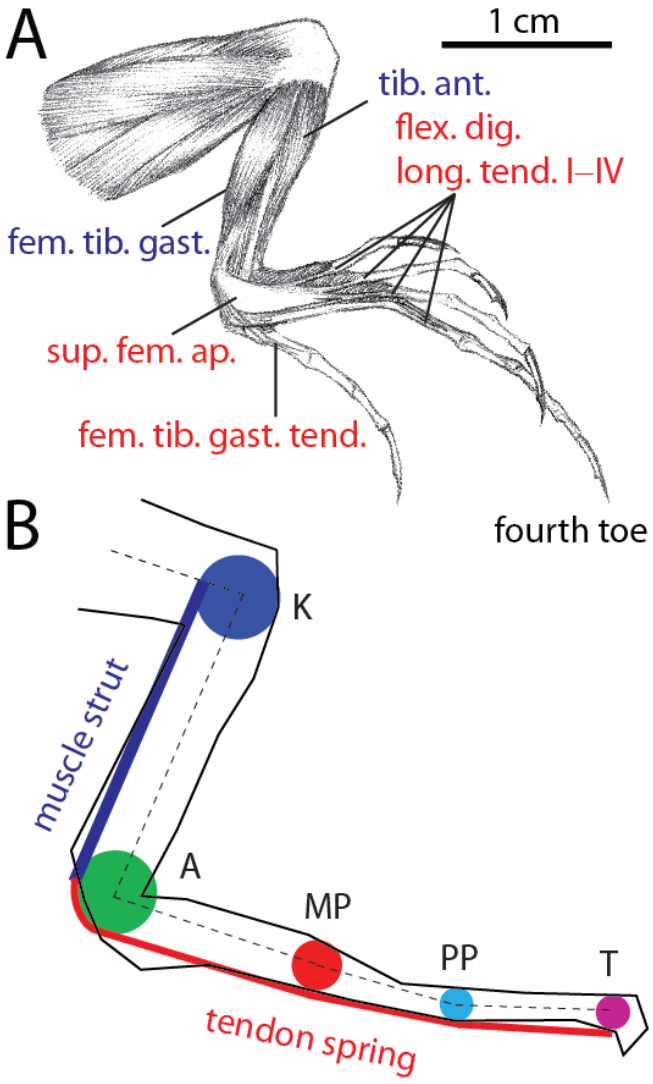

943

944 Fig. 7. Anatomy and a strut-spring model of the hind limb. (A) Ventral anatomy of a dissected
945 hind limb. Lower hind leg muscles are marked in blue; foot tendons are marked in red. (B) A
946 two-dimensional model of the hind limb. The muscle strut models isometrically contracting lower
947 leg muscles; the tendon spring models foot tendons. The radii of colored circles correspond to
948 measured joint radii.

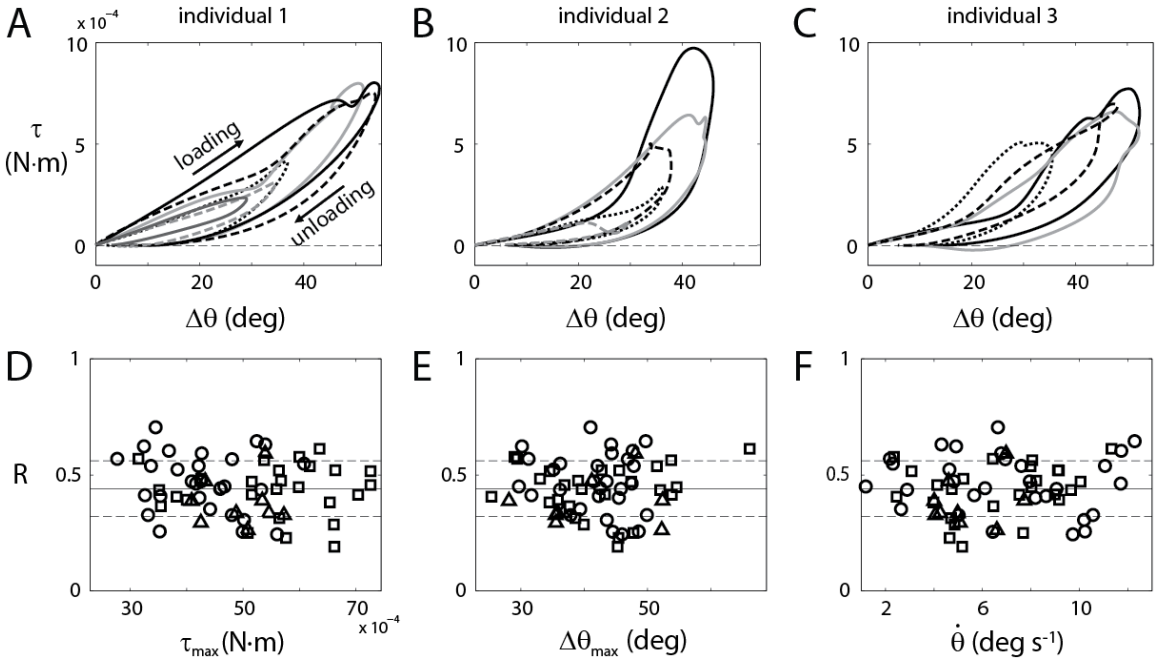

949
950

951 Fig. 8. Hind limb resilience. (A–C) Representative passive work loops of the hind foot (measured
952 at the digit tip) from each of the three anesthetized lizards tested. Different curves are from
953 different trials. The area within a work loop is the energy lost within the foot. See Fig. 2A for
954 schematic of experimental setup. (D–F) Hind limb resilience vs. maximal torque, maximal
955 angular displacement, and average loading rate. Different symbols are from different individuals.
956 Solid and dashed lines in (D–F) denote mean ± s.d.

957

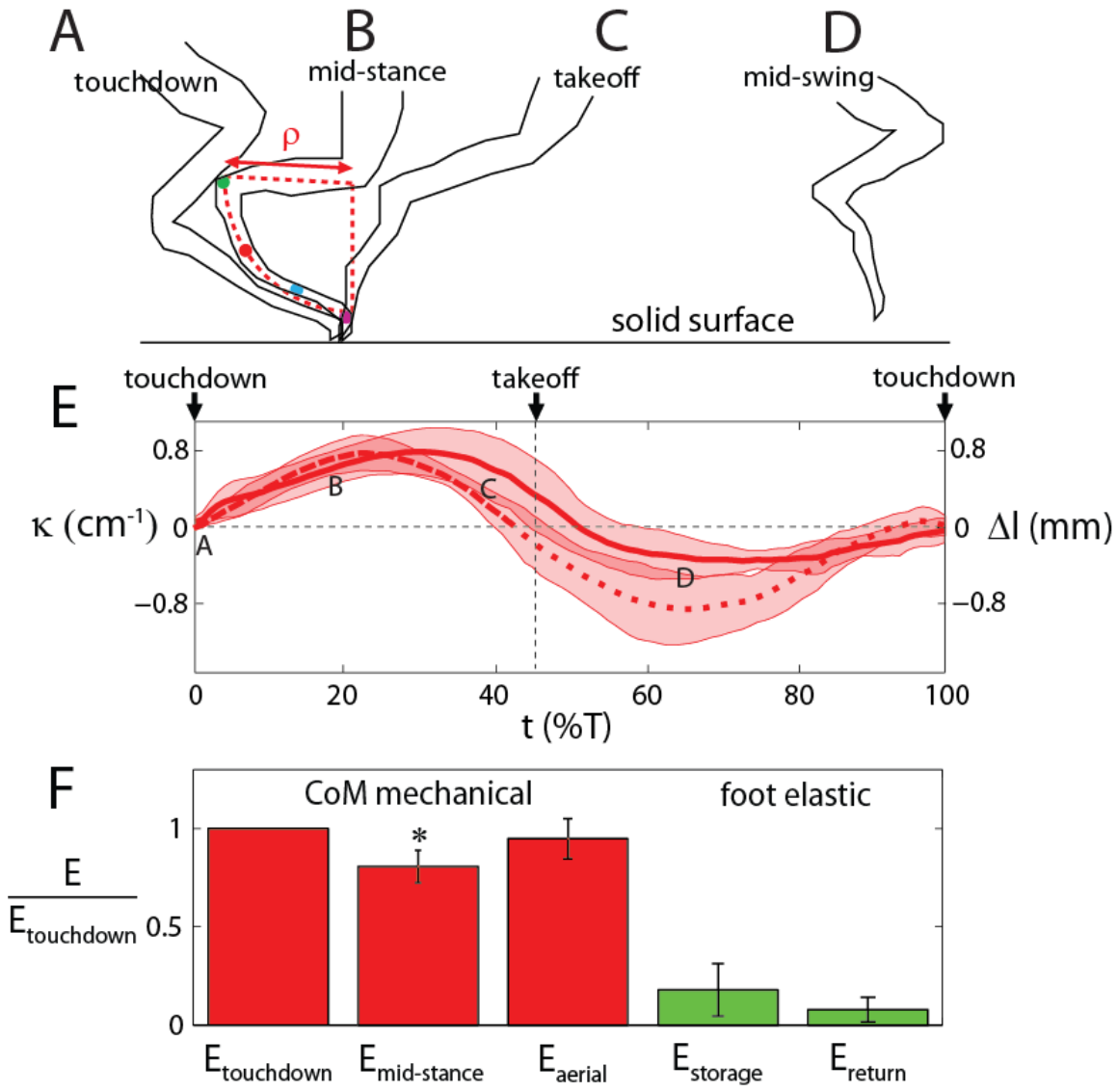

Fig. 9. Foot-ground interaction on the solid surface. (A–D) The hind foot shape from the lateral view of a representative run on the solid surface. (A–D) correspond with (A–D) in Fig. 3. The hind foot shape in the dorsal view is similar because the sprawl angle of the foot plane is nearly constant during stance. The diagram in (B) defines the radius of curvature ρ of the foot (see Appendix). (E) Foot curvature (solid) and tendon spring deformation (dashed) (mean ± s.d.) vs. time during a stride on the solid surface. Tendon spring deformation is not meaningful during swing (dotted) when the muscle strut assumption does not hold. (F) Mechanical energies of the CoM and elastic energies of the foot (mean ± s.d.) on the solid surface. All energies are normalized to the mechanical energy of the CoM at touchdown ($E_{touchdown}$) for each run. * indicates that $E_{mid\text{-}stance}$ is significantly different from $E_{touchdown}$ and E_{aerial} ($P < 0.05$, ANOVA, Tukey HSD).

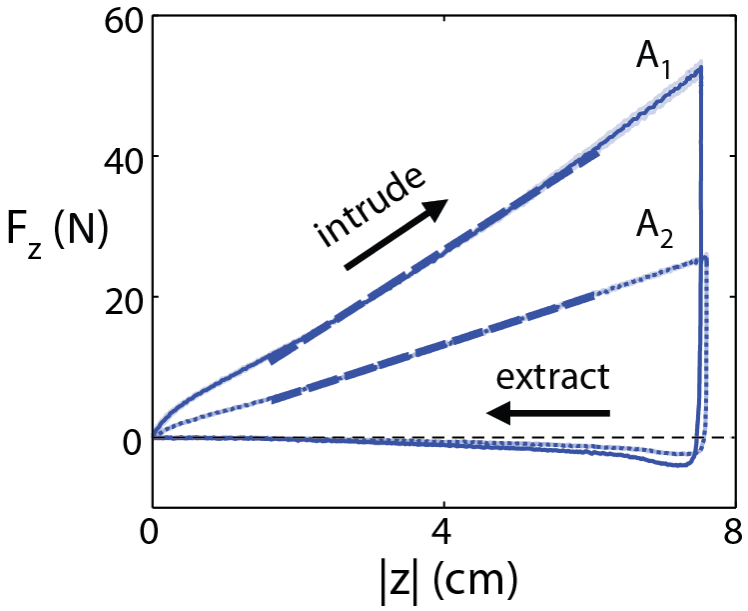

970

971 Fig. 10. Granular penetration force (mean ± s.d.) vs. depth on two plates of different areas: A_1 =
972 7.6 × 2.5 cm^2 and A_2 = 3.8 × 2.5 cm^2. See Fig. 2B for schematic of experimental setup. Dashed
973 lines are linear fits to the data over steady state during penetration using Eqn. (1).

974

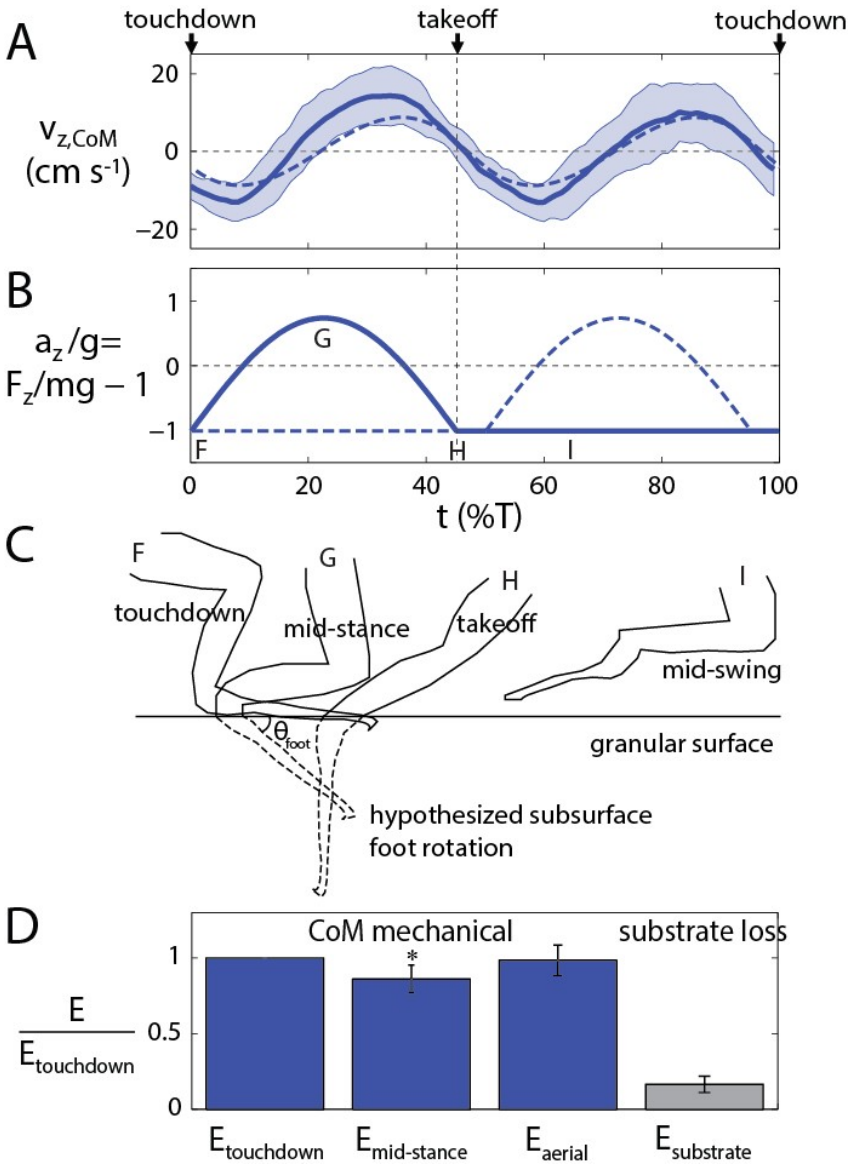

975

976 Fig. 11. Foot-ground interaction on the granular surface. (A) CoM vertical speed (mean ± s.d.) vs.
977 time during a stride. Solid curve is from experiment. Dashed curve is calculated from the vertical
978 acceleration from the model. (B) Vertical acceleration vs. time during a stride calculated from the
979 total vertical ground reaction force F_z on both feet and the animal weight mg. Solid and dashed
980 curves are the F_z on the two alternating hind feet. (C) Hypothesized subsurface foot rotation in the
981 sagittal plane. (F–I) correspond with (F–I) in Fig. 3. θ_{foot}, foot angle in the vertical plane. (D)
982 Mechanical energy of the CoM and the energy loss to the substrate (mean ± s.d.) during running
983 on the granular surface. All energies are normalized to the mechanical energy of the CoM at
984 touchdown ($E_{touchdown}$) for each run. * indicates that $E_{mid\text{-}stance}$ is significantly different from
985 $E_{touchdown}$ and E_{aerial} ($P < 0.05$, ANOVA, Tukey HSD).

986

987 Table 1. Morphological measurements (mean ± s.d.) of the seven individuals tested in the 3-D
988 kinematics experiments.

SVL (cm)	7.2 ± 0.6
Mass *m* (g)	11.0 ± 2.7
Trunk length (cm)	4.4 ± 0.4
Pelvic width (cm)	1.4 ± 0.1
Hind limb length (cm)	6.4 ± 0.1
Hind foot length (cm)	2.7 ± 0.1
Femur length (cm)	1.6 ± 0.2
Tibia length (cm)	2.1 ± 0.2
Tarsals and metatarsals length (cm)	1.0 ± 0.1
Fourth toe length (cm)	1.7 ± 0.1

989

990 Table 2. Gait and kinematic variables (mean ± s.d.) and statistics using an ANCOVA. *P* values
991 reported are for substrate effect.

Variable	Solid	Granular	*F*	*P*
†Average forward speed $\bar{v}_{x,\mathrm{CoM}}$ (m/s)	1.2 ± 0.3	1.1 ± 0.3	0.4784	0.5023
Stride frequency *f* (Hz)	7.5 ± 1.6	8.1 ± 2.0	9.9101	**0.0319**
Duty factor *D*	0.46 ± 0.05	0.45 ± 0.07	0.5032	0.5480
Stride length λ (m)	0.16 ± 0.02	0.14 ± 0.02	8.9112	**0.0409**
Average CoM height $\bar{z}_{\mathrm{CoM}}$ (cm)	3.2 ± 0.7	2.2 ± 0.5	5.4690	**0.0203**
Magnitude of CoM vertical oscillations Δz_{CoM} (cm)	0.3 ± 0.2	0.4 ± 0.3	3.7031	0.4697
Lowest CoM height z_{CoM} (cm)	3.0 ± 0.7	2.0 ± 0.4	7.7544	**0.0115**
Time of lowest CoM height (*T*)	0.18 ± 0.04	0.19 ± 0.04	0.9696	0.6366
Highest CoM height z_{CoM} (cm)	3.3 ± 0.7	2.4 ± 0.6	3.6126	**0.0447**
Time of highest CoM height (*T*)	0.44 ± 0.04	0.48 ± 0.01	3.0642	**0.0325**
Magnitude of CoM lateral oscillations Δy_{CoM} (cm)	0.86 ± 0.19	0.94 ± 0.23	0.2350	0.5263
Average pelvis height pelvis $\bar{z}_{\mathrm{pelvis}}$ (cm)	3.1 ± 0.7	1.9 ± 0.5	8.8912	**0.0046**
Average trunk pitch angle $\bar{\theta}_{\mathrm{pitch}}$ (deg)	1 ± 3	9 ± 2	19.5282	**0.0002**
Touchdown knee height z_{knee} (cm)	2.7 ± 0.7	1.7 ± 0.6	6.7157	**0.0171**
Lowest knee height z_{knee} (cm)	1.8 ± 0.5	0.7 ± 0.4	15.4261	**0.0006**
Knee vertical displacement during stance Δz_{knee} (cm)	0.9 ± 0.2	1.1 ± 0.4	0.7128	0.3056
Touchdown knee angle θ_{knee} (deg)	88 ± 25	90 ± 13	1.2344	0.6713
Lowest knee angle θ_{knee} (deg)	79 ± 17	79 ± 10	1.3175	0.7549
Highest knee angle θ_{knee} (deg)	116 ± 15	150 ± 8	17.568	**0.0001**
Knee joint extension during stance $\Delta\theta_{\mathrm{knee}}$ (deg)	37 ± 13	71 ± 4	18.0994	**0.0001**
‡Average leg sprawl angle during stance θ_{sprawl} (deg)	40 ± 1	38 ± 5	N/A	N/A
Touchdown foot angle $\theta_{\mathrm{touchdown}}$ (deg)	12 ± 4	4 ± 3	7.6973	**0.0032**

992 All significant differences ($P < 0.05$) are in bold. Degree of freedom is (2,11) for all variables.

993 † An ANOVA was used to test the effect of substrate on running speed.

994 ‡ A direct comparison was not possible for θ_{sprawl} between substrates because θ_{sprawl} was measured
995 differently: on the solid surface, leg orientation was measured from the hip to the digit tip; on the
996 granular surface, leg orientation was measured from the hip to the ankle.

997

998 Table 3. Normalized energetic variables (mean ± s.d.). All energies were normalized to $E_{touchdown}$
999 for each run and averaged over 7 representative runs on each substrate.

Variable	Solid	Granular
Mechanical energy at touchdown $E_{touchdown}$	1.00 ± 0.00	1.00 ± 0.00
Mechanical energy at mid-stance $E_{mid\text{-}stance}$	0.81 ± 0.08*	0.86 ± 0.09*
Mechanical energy during aerial phase E_{aerial}	0.95 ± 0.10	0.99 ± 0.10
Mechanical energy reduction ΔE_{mech}	0.19 ± 0.08	0.14 ± 0.09
Elastic energy storage at mid-stance $E_{storage}$	0.18 ± 0.13	N/A
Elastic energy return E_{return}	0.08 ± 0.06	N/A
Energy loss to substrate $E_{substrate}$	N/A	0.17 ± 0.05
Muscle mechanical work W_{muscle}	0.11 ± 0.10	0.31 ± 0.10

1000 * indicates significant difference ($P < 0.05$) in the mechanical energy of the CoM at mid-stance
1001 from that at touchdown and during aerial phase.